

Mid Infrared Supercontinuum Generation in Photonic Crystal Fiber

By
Redwan Ahmad

**A thesis submitted in partial fulfillment of the
requirements for the degree of**

**Master of Science
in
Communication, Multimedia and Electronics Program
in Faculty of Electrical Engineering**

**Supervisor : Prof. Dr. Stanislav Zvanovec
Co-supervisor : Dr. Matej Komanec**



**Czech Technical University in Prague
May, 2016**

Czech Technical University in Prague
Faculty of Electrical Engineering

Department of Circuit Theory

DIPLOMA THESIS ASSIGNMENT

Student: **Redwan Ahmad**

Study programme: Communications, Multimedia, Electronics
Specialisation: Systems of Communication

Title of Diploma Thesis: Mid Infrared Supercontinuum Generation in Photonic Crystal Fiber

Guidelines:

Photonic Crystal Fibers (PCFs) are suitable for supercontinuum generation because of their capability of strong modal confinement and tailorable dispersion properties to maximize bandwidth of generated optical spectrum. Based on highly nonlinear soft-glass materials, the student will design and optimize PCF with zero dispersion for supercontinuum generation in mid infrared optical region, Focus on specific shapes of PCF structures. Next step will consist of performed analyses of PCF parameters with regards to pulse duration and generated spectrum.

Bibliography/ Sources:

- [1] J. M. Dudley and J. R. Taylor, Supercontinuum generation in optical fibers. Cambridge; New York: Cambridge University Press, 2010.
- [2] G. P. Agrawal, Nonlinear fiber optics, 4th ed. Amsterdam; Boston: Elsevier / Academic Press, 2007.

Diploma Thesis Supervisor: prof. Stanislav Zvánovec Ing., Ph.D.

Co-supervisor: Ing. Matěj Komanec, Ph.D.

Valid until S 2016/2017

L.S.

prof. Ing. Pavel Pechač, Ph.d.
Head of Department

prof. Ing. Pavel Ripka, CSc.
Dean

Prague, February 19, 2016

Declaration

This is to certify that the thesis work entitled on “*Mid Infrared Supercontinuum Generation in Photonic Crystal Fiber*” by Redwan Ahmad has been carried out under my supervision as a requirement for the degree of Master of Science in Communication, Multimedia and Electronics Program in Faculty in Electrical Engineering, Czech Technical University in Prague.

Thesis supervisor

.....

Prof. Dr. Stanislav Zvánovec
Department of Electromagnetic Field
Faculty of Electrical Engineering
Czech Technical University in Prague

Co-supervisor

.....

Dr. Matěj Komanec
Department of Electromagnetic Field
Faculty of Electrical Engineering
Czech Technical University in Prague

Acknowledgement

Author wishes to express his deepest gratefulness to God Almighty Allah for the successful completion of thesis work. Special thanks to my supervisor Prof. Dr. Stanislav Zvánovec for his encouragement and valuable suggestions throughout the thesis work. It has been an honor and great pleasure for me to work under his supervision.

I would like to thank Dr. Matěj Komanec for his supervision as a co-supervisor. His valuable suggestions and directions, help me to complete thesis work successfully.

The author would like to extend his deep sense of gratitude to Tomáš Němeček for his valuable suggestions and co-operation.

It has been an honor and great achievement for me to pursue research work in wireless and fiber optics group under Faculty of electrical engineering, Czech technical university in Prague.

May, 2016
CTU, Prague

Author
Redwan Ahmad

Abstract

The main aim of this thesis is to design a simple photonic crystal fiber for supercontinuum generation in the mid-infrared region. I propose and further optimize a new photonic crystal fiber having circular ring structure by using chalcogenide glass. In next step by tailoring zero-dispersion wavelength up to 2.0 μm and 2.5 μm , supercontinuum generation obtained in the proposed photonic crystal fiber in the anomalous dispersion regime. Whole design was focused on fibers based on materials as arsenic-selenide glass and arsenic-sulfide glass, using arsenic selenide glass obtained supercontinuum broadening from 1.2 μm up to 9.0 μm . The proposed circular lattice photonic crystal fiber with ultra-wideband supercontinuum is highly desirable for purposes of spectroscopy, food quality control, pulse compression, gas sensing and various nonlinear applications. Beside this supercontinuum generation on suspended core fiber and hexagonal photonic crystal fiber based on PBG-08 glass is also analyzed. From numerical results supercontinuum spectra up to 2.5 μm based on PBG-08 glass is obtained. The effects on Supercontinuum spectra by varying peak power, pulse duration, length of PCF are studied.

Contents

1. Introduction	
1.1 Introduction to photonic crystal fiber	1
1.2 Thesis layout	3
2. Supercontinuum generation	
2.1 Introduction to supercontinuum generation	5
2.2 Applications of supercontinuum generation	7
2.3 Dispersion	8
2.4 Non-linear optics	9
2.4.1 Kerr effect	9
2.4.2 Four wave mixing	10
2.4.3 Self phase modulation	10
2.4.4 Cross phase modulation	12
2.4.5 Self- steepening	13
2.4.6 Raman scattering	13
2.4.7 Higher order solitons	14
2.5 Thesis objectives	14
3. Numerical method	
3.1 Supercontinuum generation analysis	16
3.2 Guiding properties of photonic crystal fiber	17
3.2.1 Effective mode index	17
3.2.2 Dispersion	18
3.2.3 Zero dispersion wavelength	18
3.2.4 Effective area	19
3.2.5 Non-linearity	19
3.2.6 Sech ² pulses	20
3.2.7 Peak power	20

3.2.8 Confinement loss	20
4. Design methodology	
4.1 Arsenic sulfide circular PCF	21
4.2 Arsenic selenide circular PCF	22
4.3 PBG-08 suspended core fiber	22
4.4 PBG-08 hexagonal PCF	23
4.5 Comparison of refractive index of different materials	24
4.6 Transparency range of different materials	25
5. Simulation results and discussion	
5.1 Arsenic sulfide circular lattice PCF	26
5.2 Arsenic selenide circular lattice PCF	33
5.3 PBG-08 suspended core PCF	37
5.4 PBG-08 hexagonal PCF	42
5.5 Comparison of different designs of PCF	46
6. Conclusion and future work	
6.1 Conclusion	47
6.2 Recommendations for future work	47
References	48

List of figures

Figure 1.1	Cross section view of (a) conventional optical fiber (b) photonic crystal fiber	1
Figure 1.2	Key parameters of photonic crystal fibers	2
Figure 1.3	(a) Index guiding PCF (b) PBG	2
Figure 1.4	Procedure for fabrication of photonic crystal fibers using the stack and draw method	2
Figure 2.1	A typical supercontinuum spectrum	6
Figure 2.2	White light sources	6
Figure 2.3	Dispersion curve as a function of wavelength (For single mode conventional silica glass fiber).	8
Figure 2.4	(a) $N=1$, fundamental soliton evolution (b) $N=2$ soliton evolution	11
Figure 2.5	Scheme of a SCG by fission of higher-order solitons	13
Figure 4.1	Cross section view of the proposed C-PCF	21
Figure 4.2	Cross section view of the SCF (a) 1.00 μm (b) 2.00 μm (c) 2.75 μm core diameter	23
Figure 4.3	Cross section view of the H-PCF	24
Figure 4.4	Refractive index as a function of wavelength	24
Figure 4.5	Transmission curves of selected optical fibers in the mid-IR region	25
Figure 5.1	Dispersion curve as a function of wavelength by using optimized design parameters (As_2S_3)	26
Figure 5.2	Effective area and non-linear coefficient as a function of wavelength for materials As_2S_3	27
Figure 5.3	Confinement loss as a function of wavelength (As_2S_3)	27
Figure 5.4	Dispersion curve as a function of wavelength varying pitch in case of As_2S_3	28
Figure 5.5	Spectra of broadening in As_2S_3 C-PCF using pump pulse with $T_{FWHM} = 50$ fs and (a) 1 kW peak power (b) 2 kW peak power (c) 5 kW peak power ($L_{PCF}=0.5\text{cm}$)	29
Figure 5.6	Spectra of broadening in As_2S_3 C-PCF using pump pulse with $T_{FWHM} = 50$ fs and 10 kW peak power ($L_{PCF}=0.5\text{cm}$)	30
Figure 5.7	Spectra of broadening in As_2S_3 C-PCF using pump pulse with $T_{FWHM} = 50$ fs and 2 kW peak power in different length	31
Figure 5.8	Fig. 4.8. Spectra of broadening in As_2S_3 C-PCF using pump pulse with 5 kW peak power and (a) $T_{FWHM} = 50$ fs (b) $T_{FWHM} = 100$ fs (c) $T_{FWHM} = 150$ fs ($L_{PCF}=0.5\text{cm}$)	32
Figure 5.9	Dispersion curve as a function of wavelength by using optimized design parameters (As_2S_3)	33

Figure 5.10	Effective area and non-linear coefficient as a function of wavelength for materials As_2Se_3	34
Figure 5.11	Confinement loss as a function of wavelength (As_2Se_3)	34
Figure 5.12	Dispersion curve as a function of wavelength varying air hole's diameter in case of As_2Se_3	34
Figure 5.13	Spectra of broadening in As_2Se_3 C-PCF using pump pulse with 20 kW peak power and $T_{FWHM} = 50$ fs	35
Figure 5.14	Spectra of broadening in As_2Se_3 C-PCF using pump pulse with $T_{FWHM} = 50$ fs (a) 10 kW peak power (b) 15 kW peak power	36
Figure 5.15	Dispersion as a function of wavelength for different core diameter of SCF (PBG-08)	37
Figure 5.16	Electric field distribution at 1350 nm for 2.00 μm core diameter SC-PCF.	37
Figure 5.17	SC spectra using (a) $P_{peak} = 1$ kW, $T_{FWHM} = 50$ fs for 1.00 μm core diameter SC-PCF (b) $P_{peak} = 10$ kW, $T_{FWHM} = 50$ fs for 2.00 μm core diameter SC-PCF	39
Figure 5.18	SC spectra using $P_{peak} = 10$ kW, $T_{FWHM} = 50$ fs for 2.75 μm core diameter SC-PCF	40
Figure 5.19	SC spectra using $P_{peak} = 10$ kW, $T_{FWHM} = 50$ fs for 2.75 μm core diameter SC-PCF of length (a) 1 cm (b) 5 cm (c) 10 cm (d) 15 cm.	41
Figure 5.20	Dispersion as a function of wavelength in case of H-PCF	42
Figure 5.21	Electric field distribution of H-PCF at 1560 nm (b) effective area and non-linear coefficient as a function of wavelength in case of H-PCF.	43
Figure 5.22	In the case of H-PCF, SC spectra using $T_{FWHM} = 50$ fs and P_{peak} as (a) 10 kW (b) 5 kW (c) 1 kW	44
Figure 5.23	In the case of H-PCF, SC spectra using $P_{peak} = 5$ kW with (a) $T_{FWHM} = 50$ fs (b) $T_{FWHM} = 100$ fs	45

List of tables

Table 3.1	Parameters of materials	17
Table 4.1	Non-linear refractive index (n_2) of different materials	22
Table 4.2	Design parameters of hexagonal PCF	23
Table 4.3	Transparency range of different materials	25
Table 5.1	Simulation parameters in the case of As_2S_3	28
Table 5.2	Simulation parameters in the case of As_2Se_3	35
Table 5.3	Summary of design and simulation parameters	38
Table 5.4	Summary of simulation parameters	42
Table 5.5	Broadening range by varying peak power (H-PCF)	43
Table 5.6	Broadening range by varying pulse duration (H-PCF)	45
Table 5.7	Comparison table of broadening range in different designs	46

Abbreviations

C-PCF	Circular Photonic Crystal Fiber
FEM	Finite Element Method
FWHM	Full Width at Half Maximum
FWM	Four Wave Mixing
GVD	Group Velocity Dispersion
Mid-IR	Mid-Infrared
MOF	Microstructured Optical Fiber
NLSE	Non Linear Schrödinger Equation
OCT	Optical Coherence Tomography
PBG	Photonic Band Gap
PCF	Photonic Crystal Fiber
PML	Perfectly Matched Layer
RI	Refractive Index
SC	Supercontinuum
SCF	Suspended Core Fiber
SCG	Supercontinuum Generation
SFG	Sum Frequency Generation
SHG	Second Harmonic Generation
SMF	Single Mode Fiber
SPM	Self-Phase Modulation
SRS	Stimulated Raman Scattering
SSFS	Soliton Self- Frequency Shift
THG	Third Harmonic Generation
TIR	Total Internal Reflection
XPM	Cross Phase Modulation
ZDW	Zero Dispersion Wavelength

1.Introduction

1.1 Introduction to photonic crystal fiber

Optical fibers in their simplest form achieve guidance through total internal reflection (TIR) by consisting of two regions: a high-index core and a cladding region of slightly lower refractive index (Fig. 1.1a) enabling TIR along their length. Both materials used for the core and cladding are generally fused silica with the addition of different dopants to slightly modify the refractive index [1].

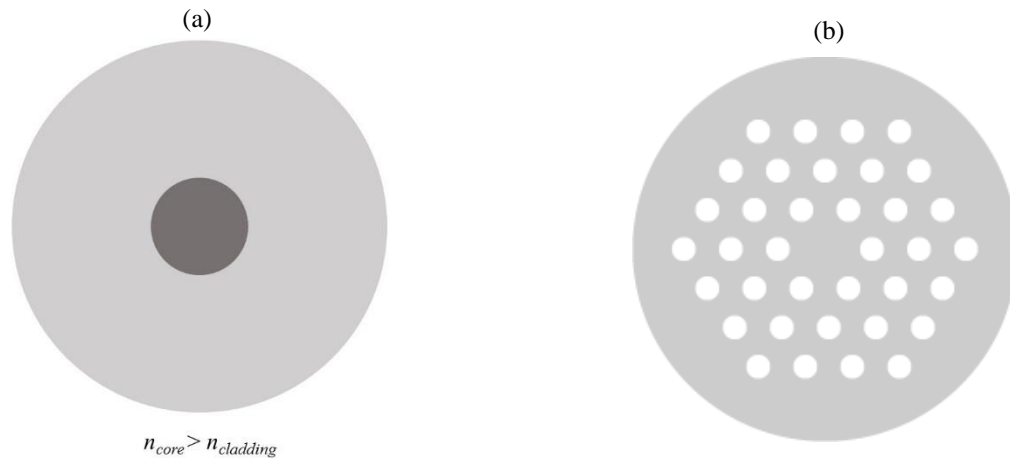


Fig. 1.1. Cross section view of (a) conventional optical fiber (b) photonic crystal fiber.

In 1996, a new kind of optical fiber was reported known as photonic crystal fiber (PCF) or microstructured optical fiber (MOF), instead of having a cladding region formed from bulk glass, had a cladding region consisting an array of microscopic air holes running along the fiber length (Fig. 1.1b). Control of the effective refractive index allows significant engineering of fiber properties such as dispersion and nonlinearity. PCFs can exhibit some unique properties which are not observed in conventional fibers such as they can support the fundamental guided mode regardless of wavelength [2]. There is a great variety of air hole arrangements, leading to PCFs with very different properties. By changing the pitch and air hole size, the dispersion and nonlinearity can be modified (see Fig. 1.2). The number of rings of air holes in the cladding is also an important quantity, impacting confinement loss. The birefringence of PCF can be modified easily by introducing two-fold symmetry to the cladding [3]. All these PCFs can be considered as specialty fibers. The simplest type of PCF has a triangular pattern of air holes, with one hole missing (see Figure 1.1b), i.e. with a solid core surrounded by an array of air holes. Most PCFs are made of pure fused silica however various PCFs made of other materials have been demonstrated, most notably of heavy metal soft glasses. Common method for PCF fabrication is stack and draw method. Procedures for fabrication are illustrated in Fig. 1.4.

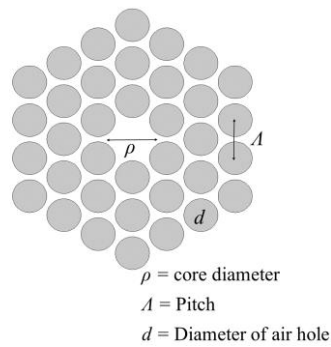


Fig. 1.2. Key parameters of photonic crystal fibers.

Photonic crystal fibers can be divided in two categories: index guiding photonic crystal fiber and photonic band gap fiber (PBG). Have a solid core like conventional fibers in index guiding PCF, light is confined in this core by exploiting the modified total internal reflection mechanism (see Fig. 1.3). In PBGs the core region has a lower refractive index than the surrounding photonic crystal cladding [8]. The light is guided by a mechanism that differs from total internal reflection in that it exploits the presence of the photonic band gap. This allows fibers to be fabricated with an air-core.

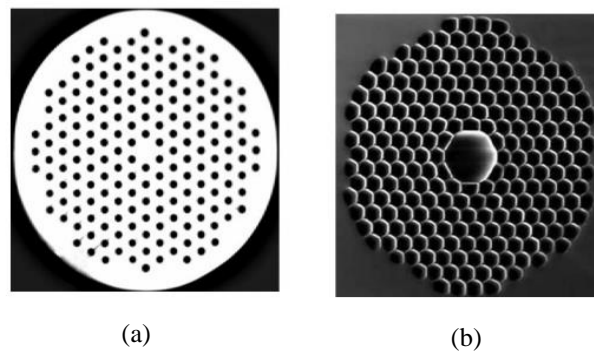


Fig. 1.3. (a) Index guiding PCF (b) PBG.

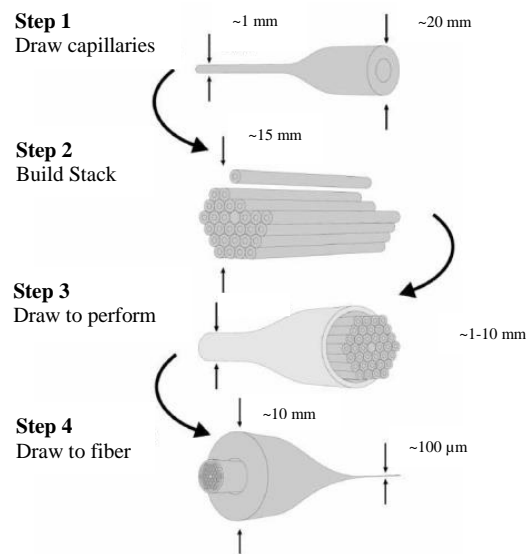


Fig. 1.4. Procedure for fabrication of PCFs using the stack and draw method.

Photonic crystal fibers have attracted much interest due to their widespread applications in optical fiber communication, nonlinear devices, optical fiber sensors, and other areas [4]-[7]. Their special properties make PCFs very attractive for a very wide range of applications.

Some examples are:

- Fiber lasers and amplifiers, including high-power devices, mode-locked fiber lasers
- Nonlinear devices such as
 - ✓ Supercontinuum generation (SCG)
 - ✓ Raman conversion
 - ✓ Parametric amplification
 - ✓ Pulse compression etc.
- Telecom components such as
 - ✓ Dispersion control
 - ✓ Filtering
 - ✓ Switching
- Fiber-optic sensors of various kinds such as
 - ✓ Temperature sensor
 - ✓ Refractive index sensor
 - ✓ Electric and magnetic field sensor
 - ✓ Gas sensor

1.2 Thesis layout

This thesis is focused on supercontinuum generation, one of the attractive applications of PCFs. Throughout the thesis I have analyzed supercontinuum generation in mid-IR regime in three different types of design with different materials. Thesis paper is divided into the following six chapters.

Chapter 1 describes general introduction about photonic crystal fiber and layout of this thesis. In chapter 2 major objectives of thesis and general introduction to supercontinuum generation and physical mechanism are described. Moreover dispersion, different non-linear phenomenon such as self-phase modulation, self-steeping, four wave mixing, Raman scattering, soliton fission etc. are also described in this chapter .

Chapter 3 includes the numerical method to calculate the guiding properties of PCF and also describing the parameters based on non-linear Schrödinger equation. Chapter 4 represents the designing process of proposed and analyzed photonic crystal fiber and used materials. Besides nonlinear refractive index and their transparency range are described in this chapter.

Chapter 5 describes analyzation of SCG broadening in the respective mid-IR region by employing our analyzed PCFs. The effects on supercontinuum spectra by varying different parameters such as peak power, pulse duration, length of PCF are studied in this chapter. Chapter 6 contains some remarkable conclusions regarding the present study and suggestions for the future work.

2. Supercontinuum generation

2.1 Introduction to supercontinuum generation

A supercontinuum source typically consists of a pulsed laser and a nonlinear element such as PCF with high non-linearity and suitable dispersion characteristics. Supercontinuum generation typically occurs when ultrashort pulses are launched into a nonlinear optical medium to yield a broadband spectrally continuous output. A typical supercontinuum spectrum is shown in Fig. 2.1. The physical mechanisms involved in this process are self-phase modulation, self-steepening, stimulated Raman scattering and four wave mixing etc. [9]. The interaction between different nonlinear processes is determined by particular parameters such as the fiber material and structure, fiber length, pump power and pump wavelength. Supercontinuum generation, first observed in 1970 by Alfano and Shapiro in bulk borosilicate glass [10]. One of the most successful application of nonlinear PCF is SCG from nanosecond, picosecond or femtosecond laser pulses. A PCF with near zero flattened chromatic dispersion around the targeted wavelength is required to generate supercontinuum (SC) with broadband flatness. PCFs are interesting candidates for SCG because of their capability of strong modal confinement and largely tailorable zero dispersion wavelength (ZDW) to maximize broadband SCG in the vicinity of a given pump wavelength.

A great variety of soft-glass fibers and pump lasers have been considered to develop the broadband mid-infrared (MIR) supercontinuum sources [11]-[14]. Due to having high material losses in silica beyond 2.5 μm , it is necessary to use non-silica glasses for SCG broadband in MIR region. Research on non-silica fibers such as tellurite glasses, chalcogenide glasses, fluoride glasses etc. has been ongoing for many years for SCG applications [15]-[19]. Compared to fluoride and tellurite glass, chalcogenide glass has more non-linear index and transparency range [20]. These glasses having high nonlinear properties about 10 to 100 times that of silica, can enhance supercontinuum generation and provide transmission window over 10 μm (chalcogenide glasses) [21]. Dispersion control is critical in that it allows greater flexibility in terms of choice of SC pump wavelength since the ZDWs of these materials are generally longer than for silica [21, 22].

The most common way to generate broadband SC in PCF using femtosecond pump pulses is to select a PCF with a ZDW which falls just below the laser wavelength. Because the dispersion is anomalous at the pump wavelength, the supercontinuum is generated by soliton dynamics. The fission of a higher order soliton produces a series of fundamental solitons which are Raman shifted to longer wavelengths, and a dispersive wave is generated at short wavelengths. This mechanism can produce a broad supercontinuum spectrum. However, soliton dynamics are extremely sensitive to pump pulse fluctuations. Small fluctuations in the pump amplitude or phase from shot to shot can cause significant fluctuations in spectral intensity and phase of the resulting supercontinuum. These fluctuations are averaged out over thousands of pulses when viewing the spectrum on a spectrometer, so the spectrum may

appear smooth, but in reality there may be large deviations from this average in each pulse. The fluctuating spectral intensity and phase translates into loss of spectral coherence. The origin of the pump fluctuations is fundamental quantum fluctuations in the laser cavity, which cannot be eradicated. Larger fluctuations due to laser technical noise can also be an issue, but can be reduced by using a less noisy laser.

When pumping below the ZDW, solitons cannot form and spectral broadening can occur only via SPM and Raman scattering. This process is less efficient and will not produce a spectrum as broad as that produced by soliton dynamics. This is due to the rapid temporal spreading of pulses under SPM and normal dispersion. The advantage of generating supercontinuum in the normal dispersion regime is that the spectral broadening is not seeded from noise, and does not amplify pump fluctuations. If some of the light generated reaches into the anomalous dispersion regime, then these frequency components will be affected by soliton dynamics. By generating supercontinuum in a PCF with an all-normal dispersion profile, thus eliminating soliton effects and reduce supercontinuum fluctuations.

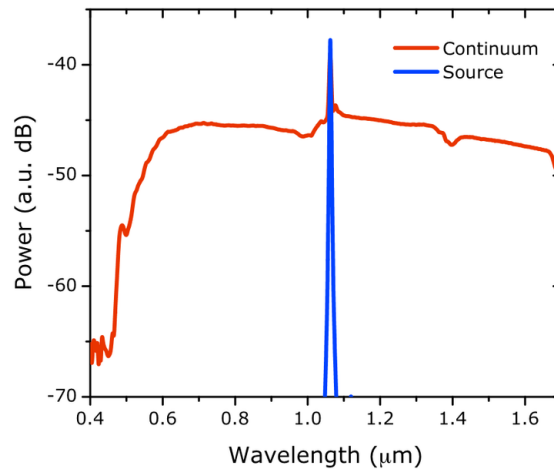


Fig. 2.1. A typical supercontinuum spectrum [36].

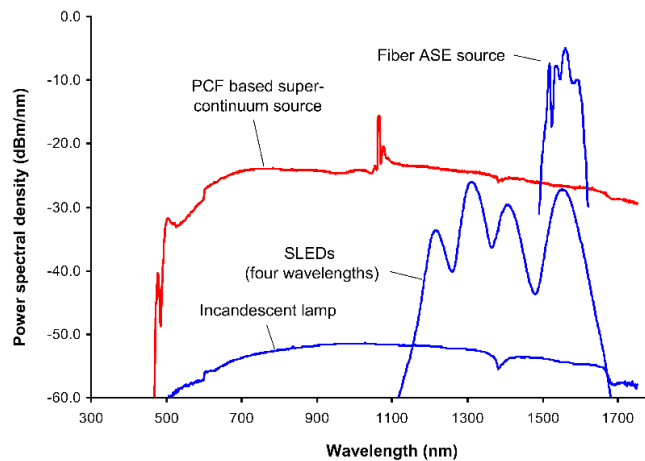


Fig. 2.2. White light sources [37].

A comparison of the bandwidth and spectrum available from different broadband light sources is shown in Fig. 2.2. PCF based supercontinuum source described here is equals or exceeds the brightness of a typical fiber coupled SLED source but offer greatly improved spectral flatness and bandwidth. Compared to PCF based SC source the ASE source power spectrum is narrower and limited to wavelengths for which suitable dopant/ host combination available. For PCF, a peak power of a kilowatts corresponding to a few tens of milliwatts of average power is sufficient to achieve complete conversion of the pump power to a broad supercontinuum.

2.2 Applications of supercontinuum generation

The most important application of the SC spectra is the replacement of white light sources which are usually tungsten-based also solve the problems of the traditional incandescent sources that is the low brightness and the coupling inefficiency to optical fibers. Most of SC sources experimentally realized have an output power in the mW range, but also higher output power have been obtained.

PCF generated SC has

- 1) High spatial coherence
- 2) Low temporal coherence

One of the most important applications of the SC sources is the optical coherence tomography (OCT) based on low coherence interferometry used in *vivo* and in *situ* cross sectional morphological imaging of transparent and non-transparent biological tissue. OCT requires has smooth spectra that variations of less than 10 dB since spectral gap can affect the image quality and the measurement precision. The spectral region between 1200 and 1500 nm is particularly important for the OCT. The SC source obtained in PCFs with slow pulses around 1060 nm are particularly promising for the OCT, because the large flat spectrum mainly generated by SRS is very stable and can be filtered in order to select the desired wavelength range.

Due to having high degree of spatial coherence SC sources are useful in spectroscopy for the fast data acquisition on small volume samples in biology, chemistry, medicine and physics.

Besides this SCG in PCF has some important potential applications in the fields such as [23]-[28].

- Ultrashort pulse compression
- Frequency metrology based on octave spinning frequency comb with fs pulses
- Lidar
- Fluorescence microscopy
- Based on low-coherence interferometry for displacement measurement and chromatic dispersion measurement in optical fibers and planar waveguides.

2.3 Dispersion

Dispersion is a linear effect but one that plays a crucial role in influencing the character of nonlinear interactions in a fiber. Dispersion arises because of the frequency variation of the effective index of the guided mode, and depends on both material and waveguide contributions.

$$D(\lambda) = -\frac{2\pi c}{\lambda^2} \beta_2 = -\frac{\lambda}{c} \frac{d^2 \text{Re}[n_{\text{eff}}]}{d\lambda^2} \quad (2.1)$$

The group velocity dispersion (GVD) β_2 and higher order dispersion terms are defined in terms of the coefficients associated with the Taylor series expansion of the propagation constant. The wavelength range where $\beta_2 > 0$ is referred to as the normal dispersion regime, whereas the wavelength range where $\beta_2 < 0$ is referred to as the anomalous dispersion regime (see Fig. 2.3), lower frequencies travel slower. The wavelength where $\beta_2 = 0$ is referred to as the zero dispersion wavelength (ZDW) and, depending on the fiber structure. Dispersion of third and higher order is called higher-order dispersion. When dealing with very broad optical spectra, one sometimes has to consider dispersion up to the fourth or even fifth and sixth order. Chromatic dispersion of second and higher order is defined via the Taylor expansion of the propagation constant β as a function of around center frequency ω_0 .

$$\beta(\omega) = \beta(\omega_0) + \beta_1(\omega_0)(\omega - \omega_0) + \frac{1}{2!}\beta_2(\omega_0)(\omega - \omega_0)^2 + \frac{1}{3!}\beta_3(\omega_0)(\omega - \omega_0)^2 + \dots \quad (2.2)$$

Dispersion has an important impact on the propagation of pulses, because a pulse always has a finite spectral width, so that dispersion can cause its frequency components to propagate with different velocities. Normal dispersion, for example, leads to a lower group velocity of higher-frequency components, and thus to a positive chirp, whereas anomalous dispersion creates negative chirps. Although dispersion alone leads to pulse broadening, dispersion combined with the Kerr nonlinearity can give rise to the formation of solitons and in this way assist the generation of extremely short pulses of light with a soliton mode-locked laser. However, this usually requires the careful management of dispersion over a wide wavelength range taking care also of higher-order terms.

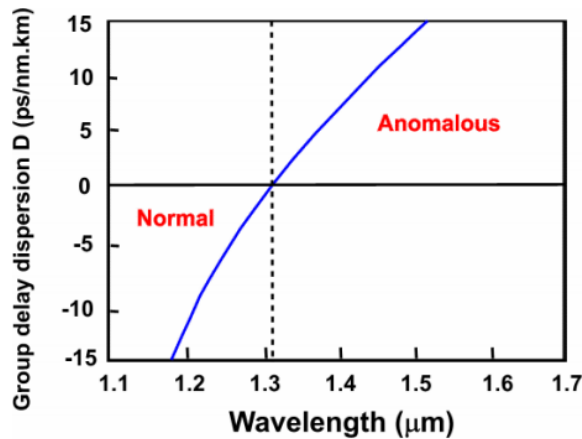


Fig. 2.3. Dispersion curve as a function of wavelength (For single mode conventional silica glass fiber).

Experimentally the group velocity dispersion can be measured by low-coherence interferometry [29].

2.4 Non-linear optics

In optics the term non-linearity refers to the relationship between the electric displacement D and the electric field E .

$$D = \epsilon_0 \epsilon_r E \quad \text{or} \quad D = \epsilon_0 E + P \quad (2.3)$$

Normally the relative permittivity ϵ_r is considered to be equivalently the electric polarization P is linearly proportional to the electric field E . In general this is not the case and to take account of nonlinear relationship between P and E can make a Taylor expansion of P in powers of E .

$$P = \epsilon_0 (\chi^{(1)} \cdot E + \chi^{(2)} \cdot EE + \chi^{(3)} \cdot EEE + \dots) \quad (2.4)$$

Where ϵ_0 is the permittivity of vacuum, E is the electric field and $\chi^{(k)}$ is the k^{th} order susceptibility. $\chi^{(1)}$ is the linear susceptibility, often contributes to the refractive index and fiber loss. $\chi^{(2)}$ is the 2nd order susceptibility which relates to nonlinear effects including second harmonic generation (SHG), sum frequency generation (SFG) etc.. However, $\chi^{(2)} = 0$ because the fiber is circular symmetric. Therefore, most nonlinear effects in silica fibers originate from the 3rd order susceptibility $\chi^{(3)}$. These include third harmonic generation (THG), four wave mixing (FWM), Kerr nonlinearity and Raman scattering.

2.4.1 Kerr effect

Kerr nonlinearity is the intensity dependence of refractive index. It is directly related to the $\chi^{(3)}$ term in the induced polarization. Given that $\chi^{(2)} = 0$ in optical fibers, the induced polarization can be re-written as

$$P = \epsilon_0 (\chi^{(1)} \cdot E + \chi^{(3)} \cdot EEE) \quad (2.5)$$

The Kerr effect is a nonlinear optical effect occurring when intense light signal propagates in crystals and glasses. The Kerr effect is the effect of an instantaneously occurring nonlinear response, which can be described as change in the refractive index of a material in response to an applied electric field. In particular, the refractive index for the high intensity light beam itself is modified according to

$$n = n_0 + n_2 I$$

(2.6)

Where $n_0 = \sqrt{1 + \chi^{(1)}}$ is the linear contribution to refractive index, n_2 is the second-order nonlinear refractive index, and I is the intensity of the wave expressed in Wm^{-2} . The refractive index change is thus proportional to the intensity of the light travelling through the medium. The n_2 value of a medium can be measured e.g. with the z-scan technique. For silica fibers, has

a nonlinear index of $\approx 2.7 \times 10^{-20} \text{ m}^2/\text{W}$. For soft glasses and particularly for semiconductors, it can be much higher, because it depends strongly on the bandgap energy. Kerr nonlinearity gives rise to many nonlinear effects, including self-phase modulation, cross phase modulation, self-steepening, modulation instability and four wave mixing.

2.4.2 Four wave mixing (FWM)

Four-wave mixing (FWM) is a third order non-linear effect caused by dependence of refractive index on the intensity of optical power. Four optical waves interact non-linearly inside a dielectric medium. Each wave passing through the medium sets up a modulation of the refractive index of the material.

If two waves with different frequencies ω_1 and ω_2 are propagating together in the medium, then the modulation of the refractive index has terms at two new frequency components given by $\omega_3 = 2\omega_1 - \omega_2$ and $\omega_4 = 2\omega_2 - \omega_1$. This process is non-degenerate FWM. The higher frequency component is known as the signal, and the low frequency component the idler. FWM is the mechanism underlying many nonlinear effects including self-phase modulation, cross phase modulation, and modulation instability.

2.4.3 Self -phase modulation (SPM)

Arising from the intensity dependent refractive index

$$n = n_0 + n_2 I \quad (2.7)$$

Where n_0 is the linear refractive index and n_2 is the nonlinear index. For silica $n_2 = 2.7 \times 10^{-20} \text{ m}^2/\text{W}$. The phase change over a fiber length L is.

$$\begin{aligned} \Delta\phi(t) &= dn.k.L = n_2 I(t)k.L \\ \Delta\omega(t) &= -\frac{d(\Delta\phi(t))}{dt} = -n_2 kL \frac{dI(t)}{dt} \end{aligned} \quad (2.8)$$

When an ultrashort pulse of light is travelling in a medium, it will induce a varying refractive index of the medium due to the optical Kerr effect. This variation in refractive index will produce a phase shift in the pulse, leading to a change of the pulse's frequency spectrum. In the context of self-phase modulation, the emphasis is on the temporal dependence of the phase shift.

When SPM occurs in a dispersive medium, qualitatively different results are obtained depending on the sign of the GVD.

Anomalous dispersion regime:

When a pulse undergoes SPM, low frequencies are generated at the leading edge, and high frequencies are generated at the trailing edge of the pulse. In the anomalous dispersion regime, the SPM induced chirp and dispersion act against one another. Newly generated frequencies move towards the pulse center, so the pulse is compressed. In some cases the dispersion and nonlinearity exactly cancel one another and produce a pulse which travels without distortion, known as a fundamental soliton. The soliton order is given by $N^2 = L_D/L_{NL}$ where L_D and L_{NL} are the characteristic dispersive and nonlinear length scales.

A fundamental soliton has soliton order $N = 1$, the dispersion length and nonlinear length are equal. A fundamental soliton propagates without any change to its temporal or spectral profile (see Fig. 2.4a). Higher order solitons have $N > 1$, and in that case SPM and dispersion are not exactly balanced. Unlike fundamental solitons they do not maintain their temporal and spectral shape during propagation (see Fig. 2.4b), and instead periodically split and re-combine over a distance known as the soliton period $z_0 = (\pi/2) L_D$.

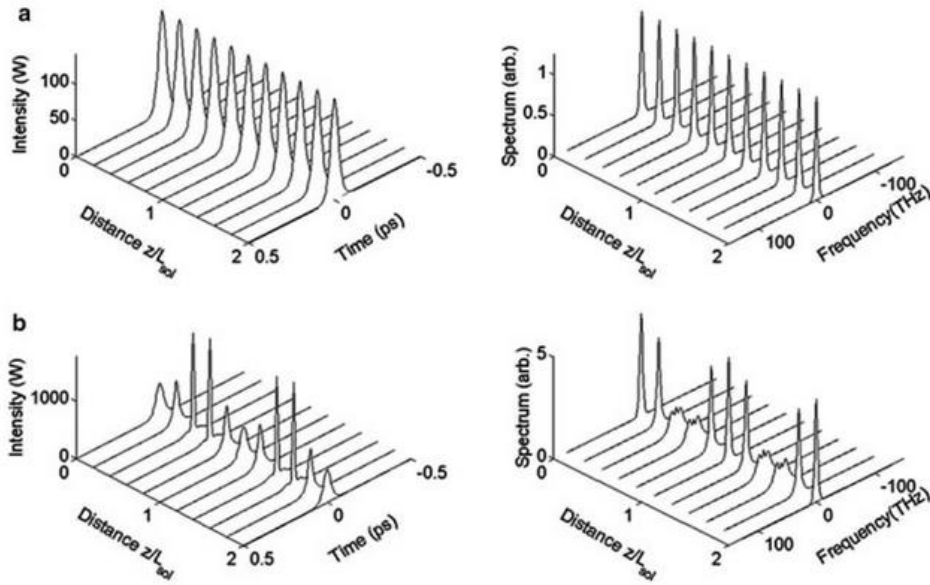


Fig. 2.4. (a) $N=1$, fundamental soliton evolution (b) $N=2$ soliton evolution. [Left side figure in time domain and right side figure in frequency domain] [38]

Soliton fission length, L_{fiss} to estimate the length at which the highest soliton compression is achieved, such that:

$$L_{fiss} = \frac{L_D}{N} = \sqrt{\frac{\tau_0^2}{|\beta_2| \gamma P_0}} \quad (2.9)$$

Where L_D is the dispersion length and N is the soliton order.

The dispersion length described by:

$$L_D = T_0^2 / |\beta_2| \quad (2.10)$$

Here T_0 is the pulse duration related with T_{FWHM} (Full width at half maximum) as $T_0 = T_{FWHM} / 1.7627$ and β_2 is the group velocity dispersion

The nonlinear length is the propagation length after which nonlinear effects become significant

$$L_{NL} = \frac{1}{\gamma P_0} \quad (2.11)$$

Where P_0 is the pulse peak power, and γ is the nonlinear coefficient.

Normal dispersion regime

Under normal GVD, the dispersion and SPM-induced chirp reinforce one another. The low frequencies generated at the leading edge of the pulse have a higher group velocity than the central frequency, and high frequencies generated at the trailing edge of the pulse have a lower group velocity. If viewing the pulse from a frame of reference moving with the pulse in time, the newly generated frequencies move away from the pulse center. The pulse broadens rapidly with propagation.

If the input pulses duration in femtosecond then self-phase modulation can lead to significant broadening which is temporally coherent. However, if the input pulses in picosecond or nanosecond then stimulated-Raman scattering tends to dominate and typically a series of cascaded discrete Stokes lines will appear until the zero dispersion wavelength is reached. At this point a soliton Raman continuum may form. As pumping in the anomalous is much more efficient for continuum generation, the majority of modern sources avoiding pumping in the normal dispersion regime.

2.4.4 Cross-phase modulation (XPM)

Cross-phase modulation (XPM) is a nonlinear optical effect where one wavelength of the propagating signal can affect the phase of another wavelength of light through the optical Kerr effect. XPM is the nonlinear modification of a light wave by another copropagating light wave with a different frequency, or polarization. Light is generated at initial frequencies ω_1 and ω_2 , and at new frequencies $2\omega_1 - \omega_2$ and $2\omega_2 - \omega_1$. The new frequency terms are only generated efficiently if there is phase matching. This is a non-degenerate four wave mixing process.

Cross-phase modulation is the change in the optical phase of a light beam caused by the interaction with another beam in a nonlinear medium, specifically a Kerr medium. This can be described as a change in the refractive index:

$$\Delta n = 2n_2 I \quad (2.12)$$

Here, the intensity I of beam 1 causes a refractive index change for beam 2. Compared with the corresponding equation for self-phase modulation, there is an additional factor of 2. This factor 2 is valid for signal with the same polarization; for cross-polarized beams in isotropic media, it must be replaced with $2/3$. A more fundamental description of cross-phase modulation effects refers to the nonlinear polarization caused in the medium, based on the $\chi^{(3)}$ nonlinearity.

2.4.5 Self-steepening

Self-steepening occurs due to the intensity dependence of the group index. The pulse peak has higher group index than the rest of the pulse, and so propagates with a lower velocity than the rest of the pulse. The result is that the intensity gradient of the leading edge is reduced, and the intensity gradient of the trailing edge is increased. If self-steepening is significant, then spectral broadening via SPM will occur asymmetrically, with increased spectral broadening on the short wavelength side of the spectrum, and higher spectral intensity on the long wavelength side to conserve energy in the FWM process. Self-steepening is more significant for shorter pulses.

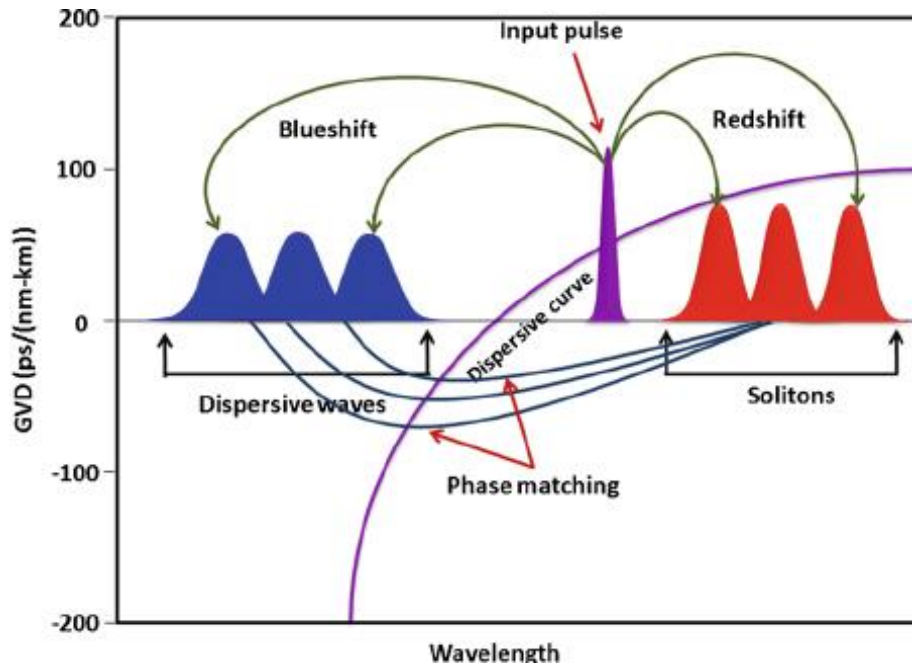


Fig. 2.5. Scheme of a SCG by fission of higher-order solitons [35].

2.4.6 Raman scattering

Raman scattering is an inelastic process, where energy is transferred to or from the material, as a result of molecular vibrational or rotational motion. In silica glass Raman scattering can occur over a broad range of frequency shifts, because the amorphous nature of the material

means the molecular vibrational frequencies form a continuum. Raman scattering is also used in spectroscopy. In particular, it allows one to investigate the vibrational modes of materials. Raman scattering can occur spontaneously, however this is a relatively weak effect. Stimulated Raman scattering is a nonlinear inelastic process in which highly efficient Raman scattering can occur under the influence of high intensity laser beam. Stimulated Raman scattering can occur within solitons whose bandwidth exceeds the Raman gain bandwidth in silica. The low frequency components experience amplification at the expense of the high frequencies, and the overall effect is that the pulse shifts to longer wavelengths. This is also known as soliton self-frequency shift (SSFS).

2.4.7 Higher order solitons

A fundamental soliton is an optical pulse which can propagate in a dispersive medium with a constant shape of the temporal intensity profile without any temporal broadening as is usually caused by dispersion. Whereas fundamental solitons are usually fairly stable, higher-order solitons can break up into fundamental solitons under the influence of various effects, such as higher-order dispersion, Raman scattering, or two-photon absorption (Fig. 2.5). Such soliton breakup sometimes plays an essential role in the process of supercontinuum generation in photonic crystal fibers. Higher order solitons decay into a series of fundamental solitons. This process is known as soliton fission. The break-up always occurs at the point of maximum compression, giving rise to a fission length L_{fiss} given by L_D/N . If a soliton is propagating close to the ZDW, then some energy can be transferred into the normal dispersion regime. This is known as a dispersive wave, and its generation requires phase matching with the Raman shifted solitons. The overall result is a broadband continuum, so this is a mechanism by which supercontinua can be generated.

2.5 Thesis objectives

In this thesis the main goal is to make a simple design which can generate SC covering mid-IR region. A great scientific effort was made to obtain broadband SC in mid-IR region [10-19], [30-34], [59]. In [30] Saini *et al.* proposed a triangular core PCF for mid-IR SCG, where due to small pitch and varying air hole's diameter in different rings the lattice design became exceedingly complex thus increasing fabrication demands. Another challenge appeared in [31] where low intensity level was present throughout the spectral broadening altogether with significant power fluctuations. In [59] authors used a 10 cm long As_2Se_3 PCF to obtain spectral broadening of up to 12 μm . Last but not least different kinds of glass such as tellurite, ZBLAN, SF57 were used to get broadband SC but due to their transparency the broadening range was limited to 4 or 5 μm [32-34].

For the first time I propose a circular PCF (C-PCF) for broadband SC by using chalcogenide glass and the pumping wavelengths for the proposed C-PCFs at 2000 nm and 2500 nm

respectively with obtained SC spectra up to 9.00 μm by using only 5 mm As_2Se_3 glass. Besides I make a manufacturing tolerance analysis of proposed C-PCFs. The reasons for selecting chalcogenide glass are wider transparency range into MIR and higher non-linear refractive index respectively. Besides chalcogenide glass I have also analyzed SCG in PCF by using PBG-08 glass. For this analysis I select two different types of PCF. One is conventional hexagonal PCF and other one is suspended-core PCF. Effects on the generated SC spectra for different PCFs are studied by changing simulation parameters such as pulse duration and peak power.

3. Numerical method

3.1 Supercontinuum generation analysis

Nonlinear propagation equations have been derived in both the time- and frequency-domains. Time-domain formulations have often been preferred because of analytic similarity to the nonlinear Schrödinger equation (NLSE) about which there is a vast literature in many fields. However, the frequency-domain formulation does show more directly the frequency-dependence of effects such as dispersion, loss and the effective mode area. Both approaches have been successfully used in the study of supercontinuum generation. Implementing the change of variable $T = t - \beta_1 z$ to transform into a co-moving frame at the envelope group velocity β_1^{-1} , a time-domain generalized NLSE for the evolution of $A(z, T)$ can be obtained [39]:

$$\frac{\partial}{\partial z} A(z, t) = -\frac{\alpha}{2} A(z, t) + \sum_{m \geq 2} \beta_m \frac{i^{m+1}}{m!} \frac{\partial^m}{\partial t^m} A(z, t) + i\gamma \left(1 + \frac{i}{\omega_0} \frac{\partial}{\partial t} \right) \left[A(z, t) \int_{-\infty}^{\infty} R(t') |A(z, t-t')|^2 dt' \right] \quad (3.1)$$

Where $A(z, t)$ is the slowly varying envelope of the electric field of the optical pulse and α represents the photonic crystal fiber loss which can be neglected since only a short length of PCF is used (depends on loss). The time derivative term on the right-hand side models the dispersion of the nonlinearity. This is usually associated with effects such as self-steepening and optical shock formation, characterized by a timescale $\tau_{\text{shock}} = \tau_0 = 1/\omega_0$. In simulation I have used hyperbolic secant pulse as input pulse as:

$$A(z = 0, t) = \sqrt{P_0} \operatorname{sech} \left(\frac{t}{T_0} \right) \quad (3.2)$$

Here T_0 is the pulse duration and related with T_{FWHM} (Full width at half maximum) as:

$$T_0 = T_{FWHM} / 1.7627. \quad (3.3)$$

Higher order dispersion coefficients:

$$\beta_m = \frac{\delta_m \beta}{\delta \omega^m} \quad (3.4)$$

Where $m=2,3,4,\dots$ represents the m^{th} order dispersion coefficients in the Taylor series expansion of the propagation constant β around the center frequency ω_0 and can be expressed as,

$$\beta(\omega) = \beta(\omega_0) + \beta_1(\omega_0) (\omega - \omega_0) + \frac{1}{2!} \beta_2(\omega_0) (\omega - \omega_0)^2 + \frac{1}{3!} \beta_3(\omega_0) (\omega - \omega_0)^3 + \dots \quad (3.5)$$

Nonlinear response function $R(t)$ can be defined as:

$$R(t) = (1 - f_R) \delta(t) + f_R h_R(t) \quad (3.6)$$

$$h_R(t) = \frac{\tau_1^2 + \tau_2^2}{\tau_1 \tau_2^2} \exp\left(-\frac{t}{\tau_2}\right) \sin\left(\frac{t}{\tau_1}\right) \quad (3.7)$$

Where f_R is the fractional contribution of the Raman response and $h_R(t)$ is the Raman response function with Raman period (τ_1) and lifetime (τ_2). The inverse time scale $1/\tau_1$ gives the phonon frequency and $1/\tau_2$ determines the bandwidth of the Lorentzian line. Parameters of glasses (f_R , τ_1 , τ_2) are summarized in Tab. 3.1.

Table 3.1
Glasses / glass materials

Material	τ_1 [fs]	τ_2 [fs]	f_R
As ₂ S ₃ [41],[42]	15.2	230.5	0.031
As ₂ Se ₃ [43],[44]	23.1	195.0	0.100
PBG-08 [45]	5.5	32	0.05
Silica [40]	12.2	32	0.18

3.2 Guiding properties of photonic crystal fiber

3.2.1 Effective mode index (n_{eff})

Efficient finite element method (FEM) using commercial full vector finite element software (COMSOL Multiphysics 5.0) is used to investigate the modal properties of the proposed C-PCF. To model the leakage and no reflection at the boundary, perfectly matched layer (PML) boundary condition is used. From Maxwell's curl equations the following vectorial equation is obtained [46].

$$\nabla \times ([s]^{-1} \nabla \times E) - k_0^2 n_{eff}^2 [s] E = 0 \quad (3.8)$$

Where E is the intensity of electric field, $[s]$ introduces the PML matrix, k_0 is the wave number in the vacuum, n_{eff} stands for the effective refractive index, the effective refractive index of the base mode is given as $n_{eff} = \beta/k_0$, where β is the propagation constant. Note that the effective refractive index depends not only on the wavelength but also on the mode in which the light propagates. For this reason, it is also called modal index. Obviously, the effective index is not just a material property, but depends on the whole waveguide design.

3.2.2 Dispersion

Dispersion is the phenomenon in which phase velocity of a wave depends on some factors such as frequency, propagation mode or polarization. Most important of these is the chromatic dispersion, which is caused by the frequency dependence of refractive index. Dispersion arises because of the frequency variation of the effective index of the guided mode, and depends on both material and waveguide contributions. Throughout the thesis consider only the chromatic dispersion of the fundamental guided mode. Chromatic dispersion is composed of material and waveguide dispersion. The total chromatic dispersion $D(\lambda)$ is calculated using the following:

$$D(\lambda) = -\frac{2\pi c}{\lambda^2} \beta_2 = -\frac{\lambda}{c} \frac{d^2 \text{Re}[n_{eff}]}{d\lambda^2} \quad (3.9)$$

Where $\text{Re}[n_{eff}]$ is the real part of the effective refractive index, c is the velocity of light and β_2 is the second order dispersion known as group velocity dispersion (GVD). Effects of fiber dispersion is usually studied by applying a Taylor expansion about a frequency ω_0 :

$$\begin{aligned} \beta(\omega) = & \beta(\omega_0) + \beta_1(\omega_0)(\omega - \omega_0) + \frac{1}{2!} \beta_2(\omega_0)(\omega - \omega_0)^2 \\ & + \frac{1}{3!} \beta_3(\omega_0)(\omega - \omega_0)^3 + \dots \end{aligned} \quad (3.10)$$

$$\text{Where } \beta_m = \left(\frac{d^m \beta}{d\omega^m} \right)_{\omega=\omega_0} \quad (3.11)$$

β_1 and β_2 are given as,

$$\beta_1 = \frac{1}{v_g} = \frac{n_g}{c} = \frac{1}{c} \left(n + \omega \frac{dn}{d\omega} \right) \quad (3.12)$$

$$\beta_2 = \frac{1}{c} \left(2 \frac{n}{\omega} + \omega \frac{d^2 n}{d\omega^2} \right) \quad (3.13)$$

Where v_g is the group velocity and n_g is the group index. β_1 is the inverse group velocity and β_2 is the GVD coefficient.

3.2.3 Zero dispersion wavelength

The zero dispersion wavelength, e.g. of an optical fiber, is the wavelength where the group delay dispersion (second-order dispersion) is zero. For PCFs with small mode areas, which can exhibit particularly strong waveguide dispersion, the zero dispersion wavelength can be shifted e.g. into the visible spectral region, so that anomalous dispersion is obtained in the visible wavelength region, allowing for, e.g., soliton transmission. Photonic crystal fibers as well as

some other fiber designs can exhibit two or even three different zero dispersion wavelengths. Supercontinuum generation can lead to particularly broad optical spectra when the pump light has a wavelength near the zero dispersion wavelength.

3.2.4 Effective area

Effective area (A_{eff}) of the analyzed PCF is evaluated based on the following equations [39]:

$$A_{eff} = \frac{\left(\iint |E|^2 dx dy\right)^2}{\left(\iint |E|^4 dx dy\right)} \quad (3.14)$$

Where E is the electric field amplitude. The integration is done not only over the core area, but over the whole plane. An important consequence of a small effective mode area is that the optical intensities for a given power level are high, so that nonlinearities become important. Also, small mode areas are usually the consequence of strong guiding, where bend losses and other effects of external disturbances are weak. If two fibers with different effective mode areas are spliced together, this will lead to some optical power loss known as splice loss. For efficiently coupling fibers with substantially different mode areas, certain mode size converters are sometimes used.

3.2.5 Non-linearity

Nonlinear coefficient of PCF represents very important parameter during SCG analysis. Nonlinear coefficient (γ) is directly proportional to nonlinear refractive index (n_2) and inversely proportional to the effective area (A_{eff}). Non-linear coefficient of the analyzed PCF are evaluated based on the following equations [39]:

$$\gamma = \frac{2\pi n_2}{\lambda A_{eff}} \quad (3.15)$$

In optical fiber technology, optical nonlinearities are of high interest. In fibers there is a particularly long interaction length combined with the high intensity resulting from a small mode area. Therefore, nonlinearities can have strong effects in fibers. Particularly the effects related to the $\chi^{(3)}$ nonlinearity – Kerr effect, Raman scattering, Brillouin scattering – are often important, despite the relatively weak intrinsic nonlinear coefficient of silica: either they act as essential nonlinearities for achieving certain functions, or they constitute limiting effects in high-power fiber lasers and amplifiers.

The non-linearity can be achieved in any fiber is limited by its mode confinement. Significant higher values of γ can be achieved by combining tight mode confinement with the use of non-silica glasses with greater intrinsic material non-linearity coefficients than silica. For transparent crystals and glasses, n_2 is typically of the order of 10^{-20} m²/W to 10^{-18} m²/W. Silica, as used e.g. in silica fibers, has a relatively low nonlinear index of 2.7×10^{-20} m²/W for

wavelengths around 1.5 μm , whereas some chalcogenide glasses exhibit several hundred times higher values. The measurement of the nonlinear index of bulk samples is often done with the z-scan technique, which is based on self-focusing via the Kerr lens.

3.2.6 Sech² pulses

Ultrashort pulses from mode-locked lasers often have a temporal shape which can be described with a squared hyperbolic secant (sech) function:

$$P(t) = P_p \operatorname{sech}^2(t/\tau) = \frac{P_p}{\cosh^2(t/\tau)} \quad (3.16)$$

The full width at half-maximum pulse duration is approximately 1.762 times the parameter τ . In many practical cases, sech² pulses have hardly any chirp, i.e., they are close to transform-limited. The time–bandwidth product is then ≈ 0.315 . The sech² shape is typical of fundamental soliton pulses. Therefore, this pulse shape also occurs in soliton mode-locked lasers.

3.2.7 Peak power

The peak power is calculated from the full width at half-maximum, FWHM pulse duration τ_p and the pulse energy E_p . The conversion depends on the temporal shape of the pulse. For example, for soliton pulses with a sech² shape the peak power is

$$P_p \approx 0.88 \frac{E_p}{\tau_p} \quad (3.17)$$

The peak power of a sech² pulse is ≈ 0.88 times the pulse energy divided by the FWHM pulse duration.

3.2.8 Confinement loss

The confinement loss is a phenomenon whereby part of the guided light penetrates to the cladding region. Confinement loss (L_c) of PCF is calculated using the following:

$$L_c = 8.686 \times \frac{2\pi}{\lambda} \operatorname{Im}[n_{eff}] \quad (3.18)$$

Where $\operatorname{Im}[n_{eff}]$ are the real part and imaginary part of the effective refractive index.

4.Design methodology

I investigate the modal properties of proposed circular lattice PCF by using two different kinds of chalcogenide glasses:

- 1) Arsenic sulfide (As_2S_3)
- 2) Arsenic selenide (As_2Se_3)

Besides I have also investigated SCG by using PBG-08 glass in following PCF:

- 1) Suspended core PCF (core diameter=1.00 μm , 2.00 μm and 2.75 μm)
- 2) Hexagonal PCF

4.1 Arsenic sulfide circular PCF

I investigated SCG by introducing circular PCF (C-PCF) structure. Figure 4.1 illustrates the cross sectional view of the proposed C-PCF. It contains four rings, each having $8 \times n$ number of air holes (where $n = 1, 2, 3, 4$ introduces number of rings). Optimized parameters for proposed PCFs are: $A = 1.9 \mu\text{m}$, $d = 1.3 \mu\text{m}$ and core diameter ($2 \times (A - d/2)$) = 2.5 μm , respectively. Here d stands for the diameter of each air hole and A is the pitch of the lattice. Diameter of all air holes in different rings kept equal, which makes design simple and will reduce fabrication complexity. The proposed design can be then fabricated e.g. by using conventional stack and draw technique [47].

The refractive indexes of chalcogenide glass As_2S_3 are determined using the Sellmeier equation:

$$n(\lambda) = \sqrt{1 + \frac{B_1\lambda^2}{\lambda^2 - C_1^2} + \frac{B_2\lambda^2}{\lambda^2 - C_2^2} + \frac{B_3\lambda^2}{\lambda^2 - C_3^2} + \frac{B_4\lambda^2}{\lambda^2 - C_4^2} + \frac{B_5\lambda^2}{\lambda^2 - C_5^2}} \quad (4.1)$$

Where Sellmeier coefficients of As_2S_3 glass are $B_1=1.898367$, $B_2=1.922297$, $B_3=0.87651$, $B_4=0.11887$, $B_5=0.95699$, $C_1=0.15$, $C_2=0.25$, $C_3=0.35$, $C_4=0.45$ and $C_5=27.3861$ [48], [51].

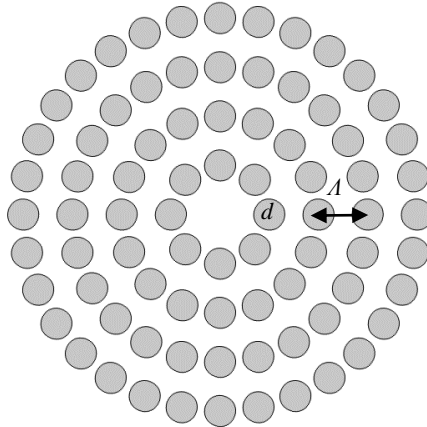


Fig. 4.1. Cross section view of the proposed C-PCF.

4.2 Arsenic selenide circular PCF

The refractive indexes (RI) of As_2Se_3 are then determined using the equation proposed by Thompson for amorphous material [50] as:

$$n(\lambda) = \sqrt{1 + \lambda^2 \left(\frac{A_0^2}{\lambda^2 - A_1^2} + \frac{A_2^2}{\lambda^2 - 19^2} + \frac{A_3^2}{\lambda^2 - 4A_1^2} \right)} \quad (4.2)$$

Where As_2Se_3 glass Sellmeier coefficients are $A_0= 2.234921$, $A_1= 0.24164$, $A_2= 0.347441$ and $A_3= 1.308575$ [49],[50]. For analyzing the modal properties of the proposed C-PCF I have used the same PCF design parameters in the case of As_2Se_3 ($A = 1.9 \mu\text{m}$, $d = 1.3 \mu\text{m}$).

4.3 PBG-08 suspended core fiber

Figure 4.2 illustrates the cross sectional view of the analyzed SCF. I have analyzed SCG by using suspended core PCF (SC-PCF) of 3 different core diameter as $1.00 \mu\text{m}$, $2.00 \mu\text{m}$ and $2.75 \mu\text{m}$ respectively. The radius r_1 , r_2 and r_3 of three different core diameter SCF are $24.5 \mu\text{m}$, $24 \mu\text{m}$ and $23.625 \mu\text{m}$ respectively and bridge width w_1 , w_2 and w_3 are $0.4 \mu\text{m}$, $1.0 \mu\text{m}$ and $1.6 \mu\text{m}$ respectively (see Fig. 4.2). As a material I have used PBG-08 glass. Transmission window of PBG-08 in the range of $0.5 - 4.8 \mu\text{m}$ [52]. The non-linear refractive index of PBG-08 is $4.3 \times 10^{-19} \text{ m}^2/\text{W}$ using z-scan method at the wavelength 1240 nm . Due to having tight confinement along the core, SC-PCF exhibits high non-linearity, which make broader spectra. The refractive indexes of PBG-08 glass is determined using the following Sellmeier equation.

$$n(\lambda) = \sqrt{1 + \frac{B_1 \lambda^2}{\lambda^2 - C_1} + \frac{B_2 \lambda^2}{\lambda^2 - C_2} + \frac{B_3 \lambda^2}{\lambda^2 - C_3}} \quad (4.3)$$

For PBG-08 glass Sellmeier coefficients are $B_1= 2.01188143$, $B_2= 0.54673236$, $B_3= 1.39488613$, $C_1= 0.01537572$, $C_2= 0.06355233$ and $C_3= 141.65404618$ [52]. The non-linear refractive index for different materials are listed in Tab. 4.1.

Table 4.1
Non-linear refractive index (n_2) of different materials

Material	Non-linear refractive index (n_2) [m^2/W]
As_2S_3 [48,51]	3.0×10^{-18}
As_2Se_3 [49-50]	2.4×10^{-17}
PBG-08 Glass [52]	4.3×10^{-19}
Silica	2.7×10^{-20}

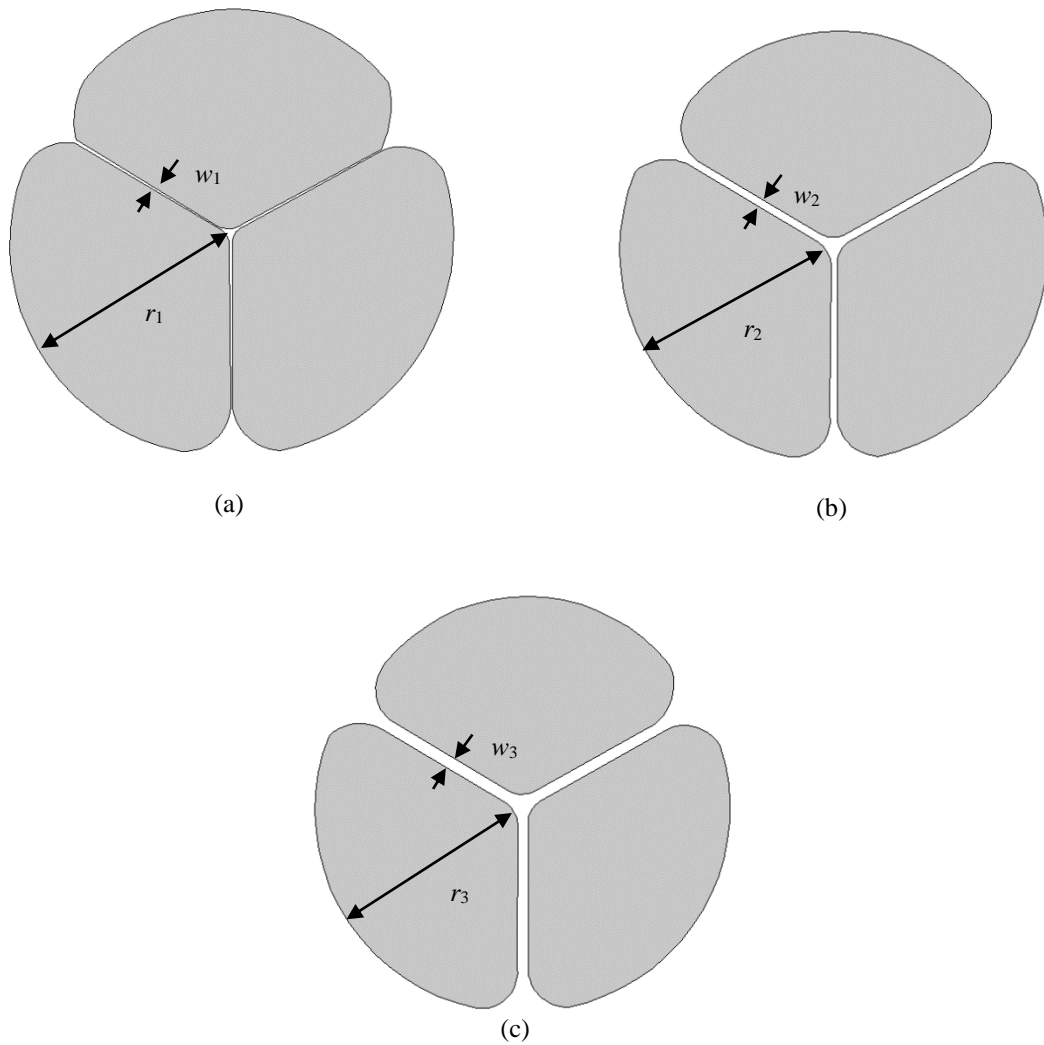


Fig. 4.2. Cross section view of the SCF (a) 1.00 μm (b) 2.00 μm (c) 2.75 μm core diameter.

4.4 PBG-08 hexagonal PCF

Figure 4.3 illustrates the cross sectional view of the analyzed hexagonal PCF. I have analyzed SCG by using H-PCF of following parameters. PBG-08 glass is used as a host material.

Table 4.2

Design parameters of hexagonal PCF

Pitch	2.32 μm
Diameter of air hole (d)	2.00 μm
Core diameter	2.64 μm
Number of. Rings	7

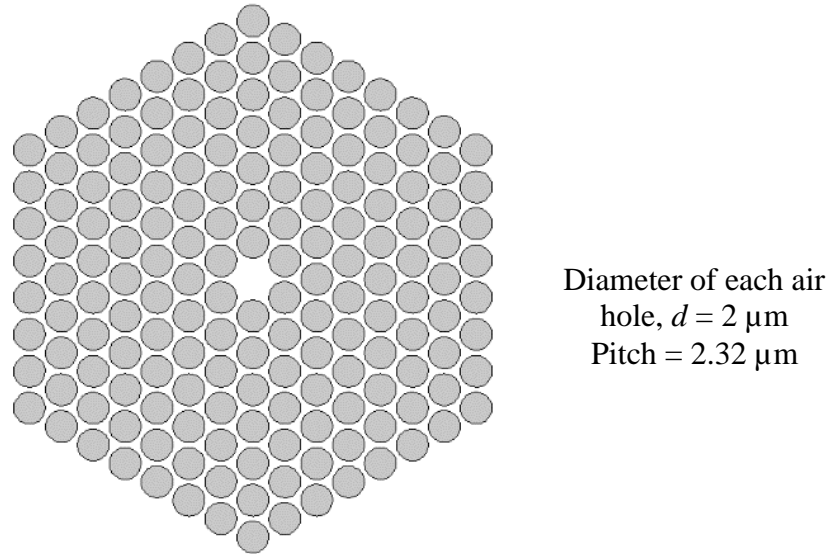


Fig. 4.3. Cross section view of the H-PCF.

4.5 Comparison of refractive index of different materials

Comparison of refractive indexes of different materials such as As_2S_3 , As_2Se_3 and PBG-08 glass are shown in Fig. 4.4. From curve it is seen that chalcogenide glass (As_2Se_3) has larger refractive index compared to As_2S_3 glass and PBG-08 glass. For As_2Se_3 , at 2500 nm the refractive index is 2.7978.

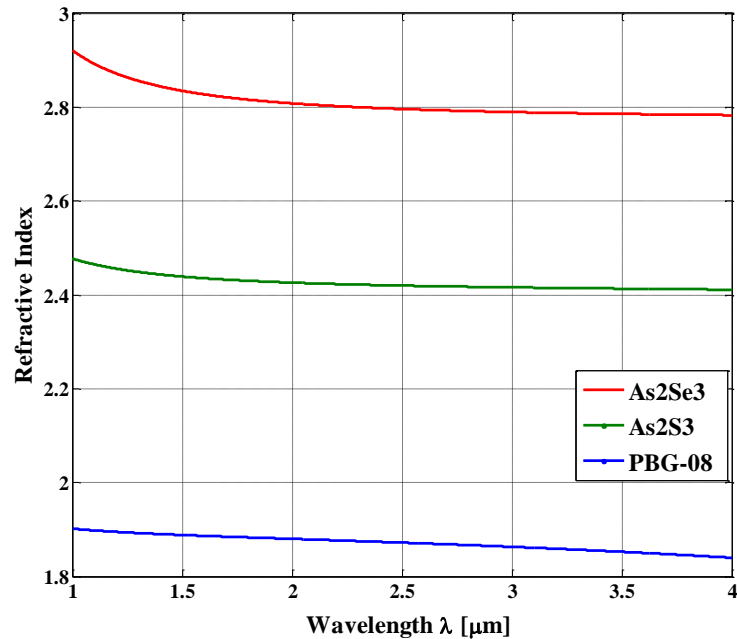


Fig. 4.4. Refractive index as a function of wavelength.

4.6 Transparency range of different materials

Transparency range for different materials are described in Tab. 4.2. Soft glasses, or compound glasses, are defined as glasses which have lower melting and processing temperatures than those of silica. Soft glasses can be classified into three categories: oxides, fluorides and chalcogenides [57,58]. There are some important advantages of soft glasses over silica such as, they allow transmission of light in the IR, a wavelength range that is of great interest for applications in mid-IR spectroscopy (see Fig. 4.5), LIDAR and material processing [57,58]. Along with their Kerr nonlinearity coefficient can be three orders of magnitude higher than that of silica glass. Finally, their typical melting temperature is in the 200-1000°C range (depending on glass composition), much lower than that of silica (1800-2300°C), potentially facilitating the fabrication process.

Table 4.3
Transparency range of different materials

Name	Range
Silica	0.4-2.4 μm
PBG-08 glass [52]	0.5-4.8 μm
Tellurite glass (Zn-TeO ₂)[54]	0.4-5.0 μm
Arsenic sulfide (As ₂ S ₃)[55]	0.7-7.0 μm
Arsenic selenide (As ₂ Se ₃)[55]	1.0-9.0 μm
Fluoride glass (ZBLAN) [56]	0.3-4.8 μm

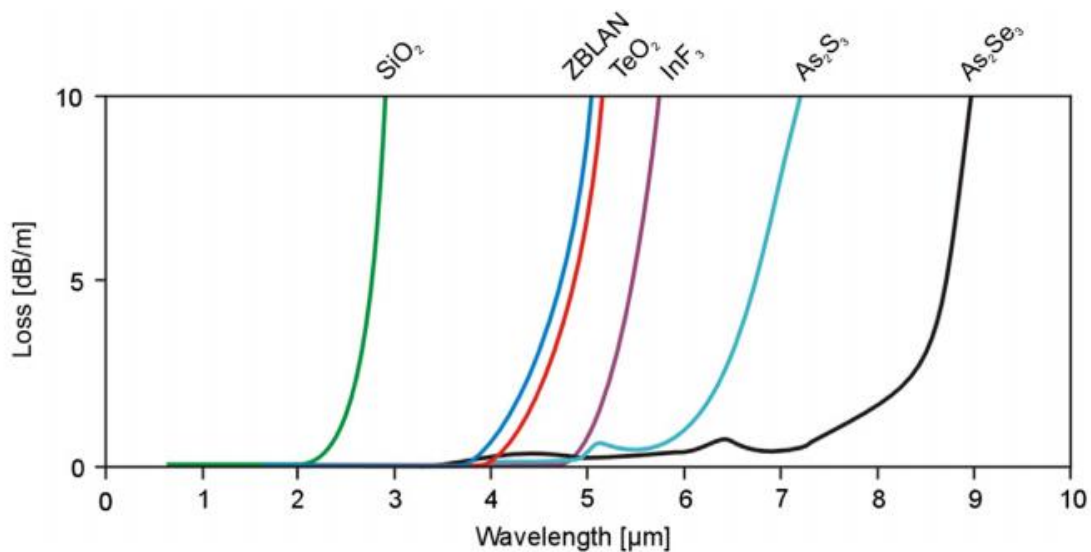


Fig. 4.5. Transmission curves of selected optical fibers in the mid-IR region [53].

5. Simulation results and discussion

5.1 Arsenic sulfide circular lattice PCF

In the case of chalcogenide glass material As_2S_3 , the wavelength dependent dispersion, effective mode area (A_{eff}) of propagating mode, confinement loss and corresponding nonlinear coefficient (γ) are illustrated in Fig. 5.1-5.3. From Fig. 5.1a it can be seen that ZDW of the proposed C-PCF (As_2S_3) is 1985 nm and pumping wavelength chosen in the anomalous dispersion regime. The electric field distribution of C-PCF (As_2S_3) at 2000 nm is shown in Fig. 5.1b. For SCG analysis chosen pumping wavelength as 2000 nm, where the proposed C-PCF offers $\gamma = 2362 \text{ W}^{-1}\text{km}^{-1}$ and $A_{eff} = 3.989 \mu\text{m}^2$ (Fig. 5.2).

By taking $\lambda = 2000 \text{ nm}$ as the pumping wavelength of the input pulse the calculated dispersion coefficient values of the Taylor expansion are $\beta_2 = -1.07 \times 10^{-2} \text{ ps}^2/\text{m}$, $\beta_3 = 1.4566 \times 10^{-3} \text{ ps}^3/\text{m}$, $\beta_4 = -3.9289 \times 10^{-6} \text{ ps}^4/\text{m}$, $\beta_5 = 2.113 \times 10^{-8} \text{ ps}^5/\text{m}$, $\beta_6 = -1.2547 \times 10^{-10} \text{ ps}^6/\text{m}$, $\beta_7 = 8.5047 \times 10^{-13} \text{ ps}^7/\text{m}$, $\beta_8 = -5.6878 \times 10^{-15} \text{ ps}^8/\text{m}$, $\beta_9 = 1.51 \times 10^{-17} \text{ ps}^9/\text{m}$ and $\beta_{10} = 6.5143 \times 10^{-19} \text{ ps}^{10}/\text{m}$.

Confinement loss (L_c) of proposed C-PCF is simulated (Fig. 5.3) by using As_2S_3 material and up to wavelength 5000 nm negligible confinement loss exists only material loss dominates during broadening of SCG. Though, only PCF of 0.5 cm length is used here, so the effect of losses in the broadening of SCG can be omitted.

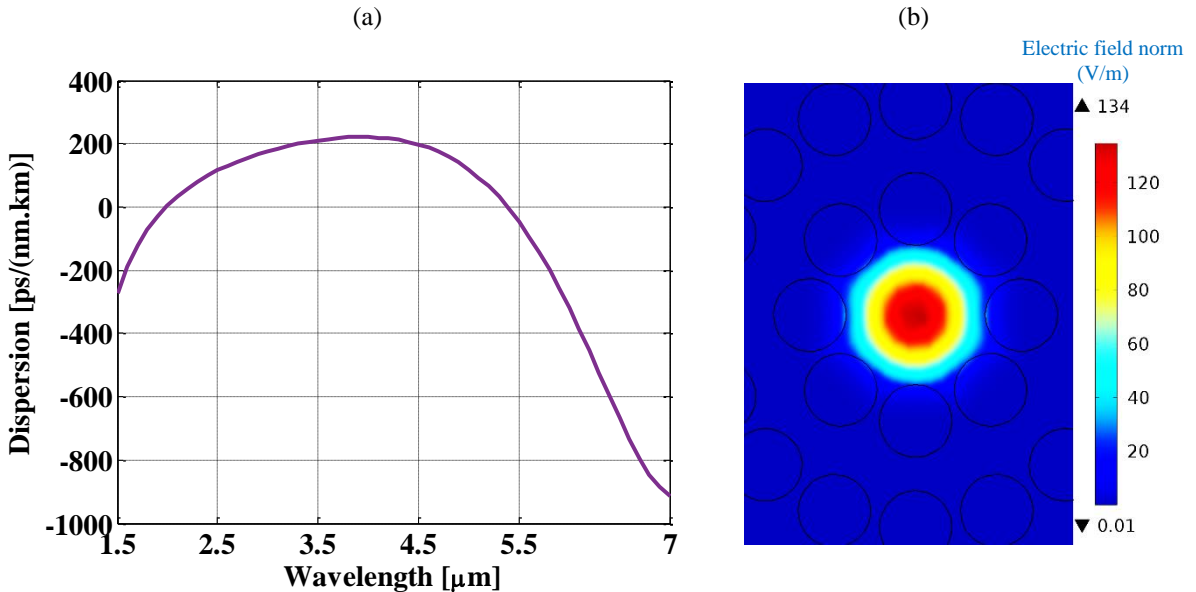


Fig. 5.1. (a) Dispersion curve as a function of wavelength by using optimized design parameters (As_2S_3) (b) Electric field distribution of C-PCF (As_2S_3) at 2000 nm.

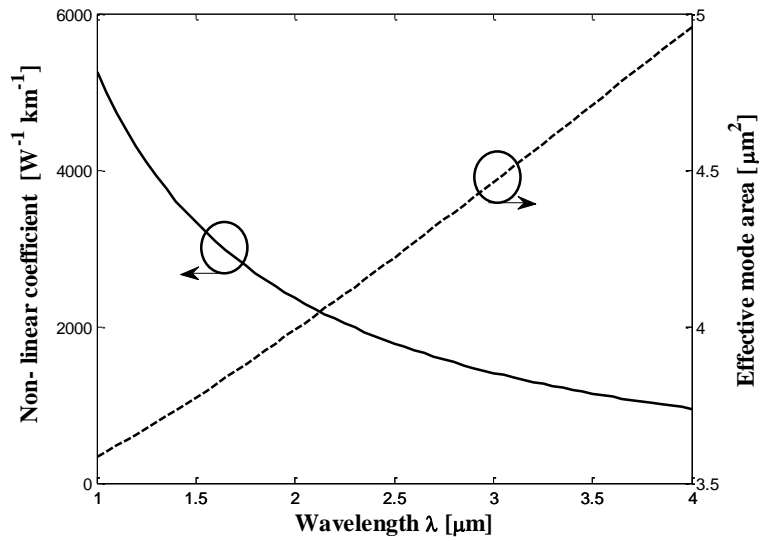


Fig. 5.2. Effective area and non-linear coefficient as a function of wavelength for materials As_2S_3 .

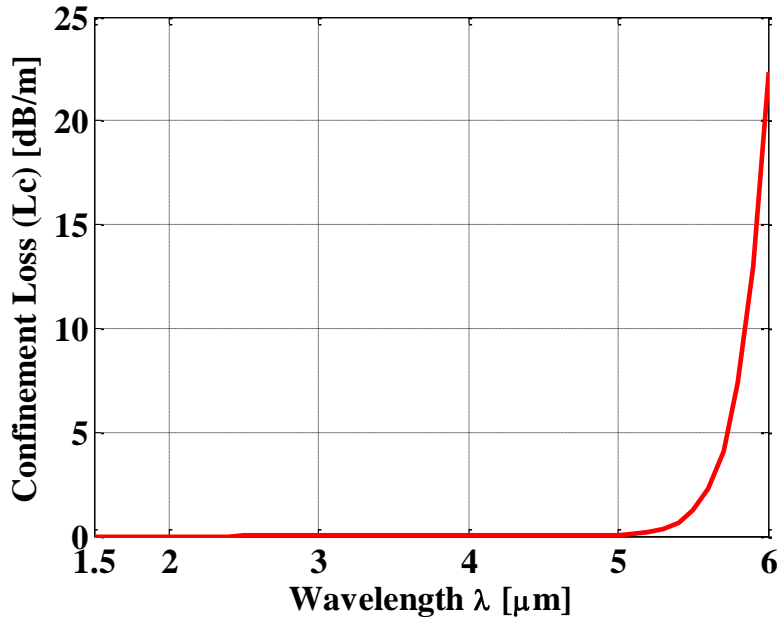


Fig. 5.3. Confinement loss as a function of wavelength (As_2S_3).

During fabrication, we have to expect tolerance of $\pm 2\%$ from designed parameters of proposed C-PCF [62]. That is why I perform in next step a tolerance analysis on proposed C-PCF by varying pitch. In As_2S_3 C-PCF I vary pitch ($A = 1.8, 1.9$ and $2.0 \mu m$) keeping the diameter of air holes fixed. From Fig. 5.4 it is clear that we cannot experience such a significant change on dispersion curve while varying pitch; dispersion of proposed structure proved to be less sensitive to the structural parameters changes.

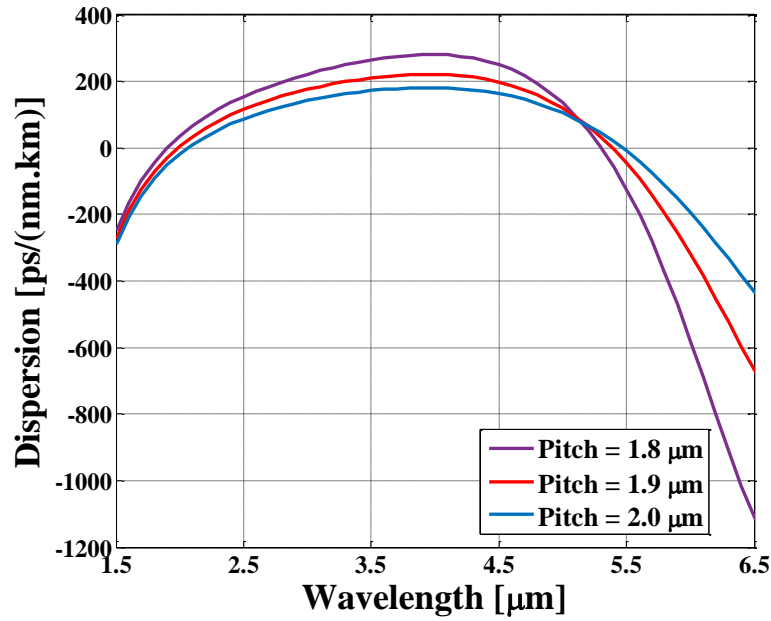


Fig. 5.4. Dispersion curve as a function of wavelength varying pitch in case of As_2S_3 .

Table 5.1

Simulation parameters in the case of As_2S_3

Parameters	Value
Pumping wavelength	2000 nm
Zero dispersion wavelength	1985 nm
Non – linear coefficient (γ)	At 2000 nm = $2362 \text{ W}^{-1}\text{km}^{-1}$
Fractional Raman contribution (f_R)	0.031
Raman response parameters	$\tau_1 = 15.2 \text{ fs}$, $\tau_2 = 230.5 \text{ fs}$
Length of PCF (L_{PCF})	0.5 cm

Simulation parameters for optimized SCG in the case of As_2S_3 are shown in Tab. 5.1. In simulation I have selected hyperbolic secant pulse as input pulse with peak power of 1 kW, 2 kW, 5 kW and 10 kW respectively. From simulation results it is seen that by using peak power 10 kW and $T_{FWHM} = 50 \text{ fs}$ observed spectral broadening is about 3000 nm, from 1100 nm to 4100 nm (Fig. 5.6). And by using peak power of 1 kW, 2 kW and 5 kW, obtained spectral broadening about 1300 nm (Fig. 5.5a), 1700 nm (Fig. 5.5b) and 2200 nm (Fig. 5.5c) respectively. In all above cases, only 0.5 cm long PCF is employed with $T_{FWHM} = 50 \text{ fs}$. From simulation results it can be seen that as peak power increases from 5 kW to 10 kW, there is a very small change in spectral broadening. For pumping at 2000 nm, mode locked thulium fiber laser can be used [14],[60],[61].

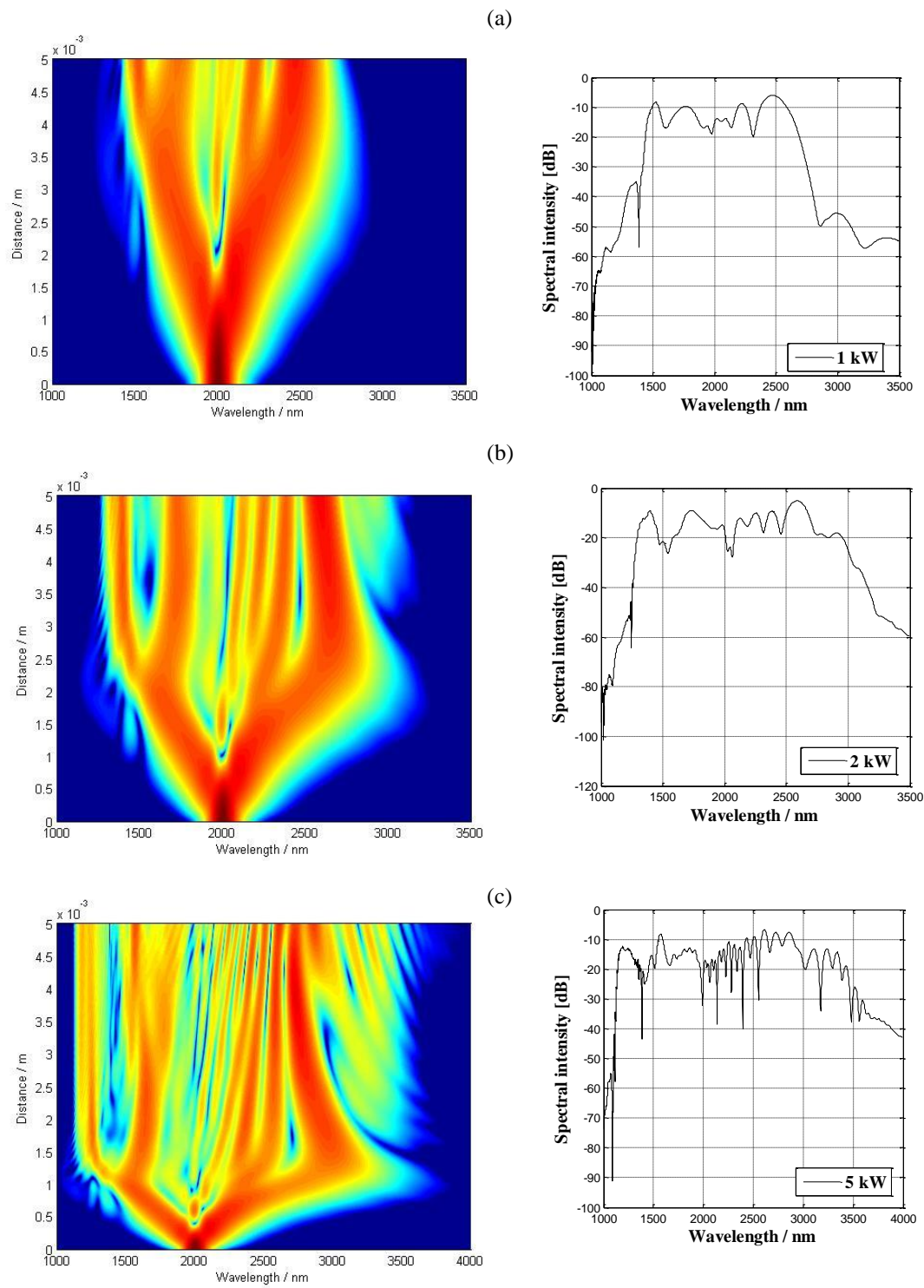


Fig. 5.5. Spectra of broadening in 0.5 cm long As_2S_3 C-PCF using pump pulse with $T_{FWHM} = 50$ fs and (a) 1 kW peak power (b) 2 kW peak power (c) 5 kW peak power.

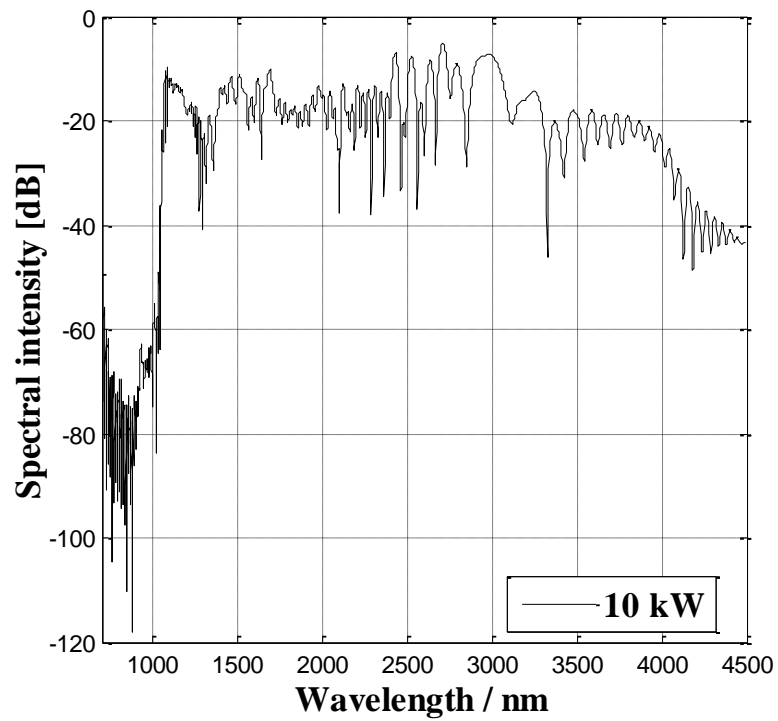
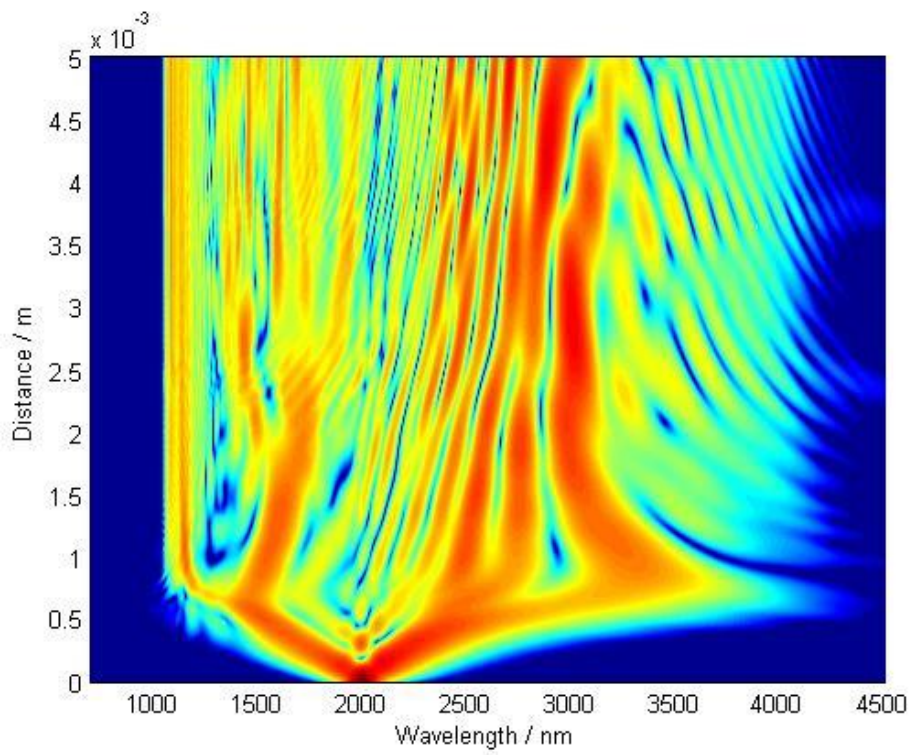


Fig. 5.6. Spectra of broadening in 0.5 cm long As_2S_3 C-PCF using pump pulse with $T_{FWHM} = 50$ fs and 10 kW peak power.

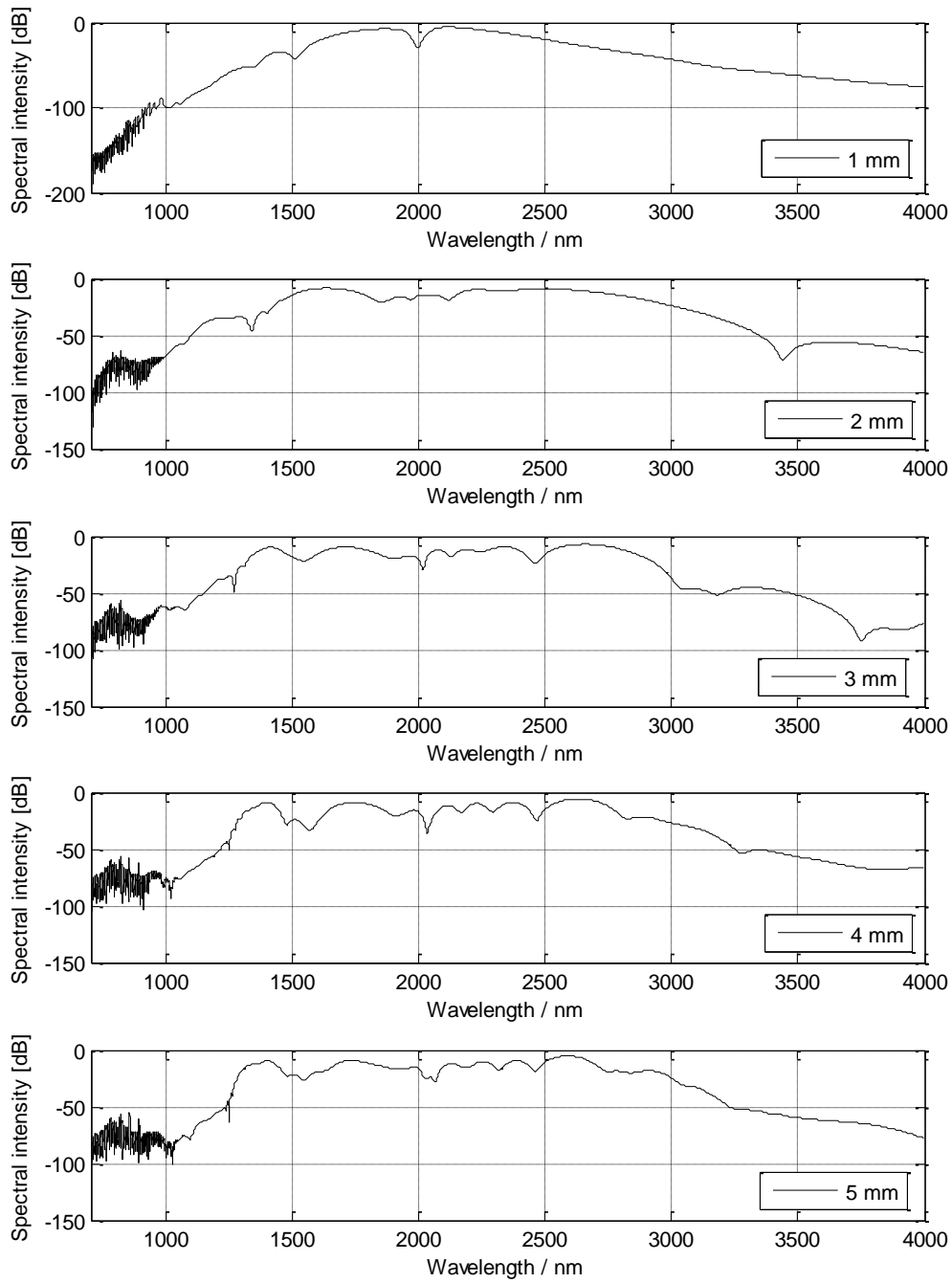


Fig. 5.7. Spectra of broadening in As_2S_3 C-PCF using pump pulse with $T_{FWHM} = 50$ fs and 2 kW peak power for different C-PCF lengths.

Non-linear length ($L_{NL}=1/\gamma P_0$) and dispersion length ($L_D=T_0^2/|\beta_2|$) of the proposed C-PCF by using As_2S_3 material are 4.23×10^{-5} m and 7.5×10^{-2} m respectively (using $P_0=10$ kW and $T_0=0.0284$ ps) at 2000 nm pumping wavelength. So the non-linear effects play a significant role initially in spectral broadening. By fulfilling the conditions as ($L_{NL}<L_D$) and ($L_{NL}<L_{PCF}$) [9], the non-linear effect is dominant here and initially self - phase modulation (SPM) leads to a symmetric spectral broadening of input pulse. The effect of varying pulse duration on broadening is shown in Fig. 5.8 by using peak power as 5 kW. I have analyzed broadening in SCG by using pulse duration T_{FWHM} as 50 fs, 100 fs and 150 fs respectively. From simulation results it is seen that as the pulse duration increases, starting length of broadening is shifted with a slight increases. In all above cases spectral broadening range is same with different intensity level.

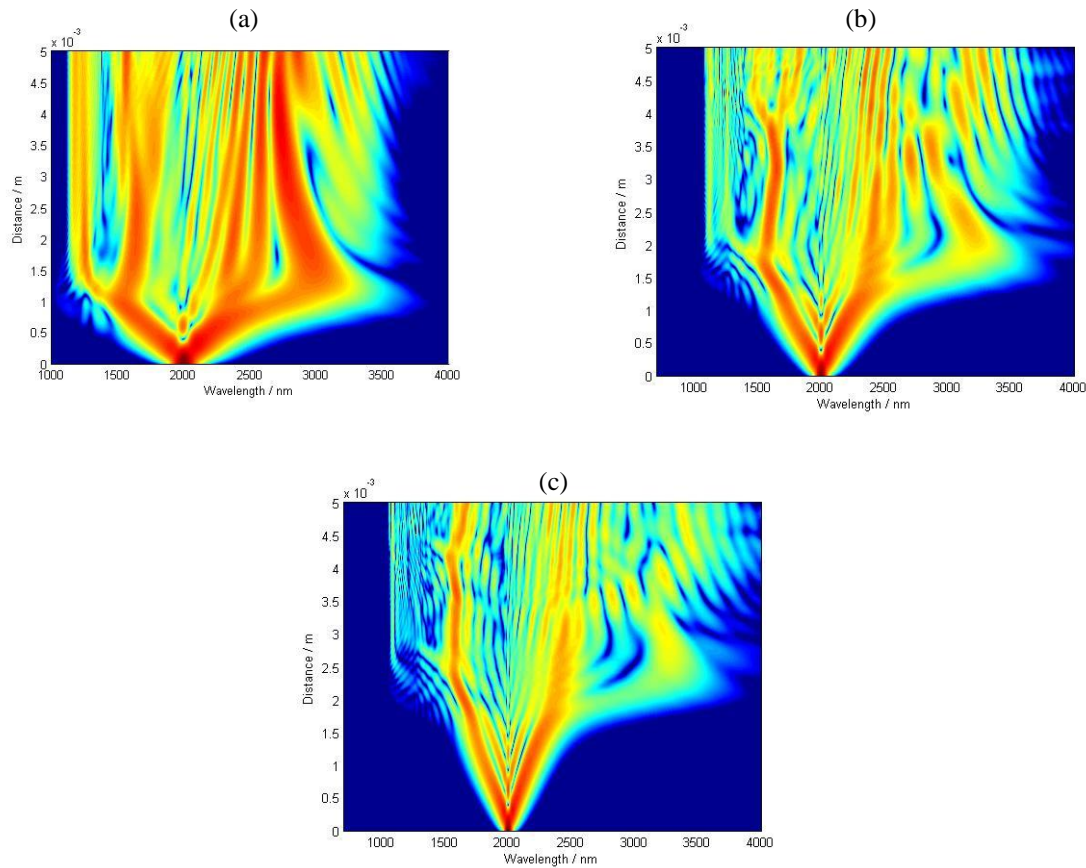


Fig. 5.8. Spectra of broadening in 0.5 cm long As_2S_3 C-PCF using pump pulse with 5 kW peak power and (a) $T_{FWHM} = 50$ fs (b) $T_{FWHM} = 100$ fs (c) $T_{FWHM} = 150$ fs.

From Fig. 5.5(a-c) it is seen that the SC spectra consists of some ripples because of SPM as non-linear length is much smaller than dispersion length. For low peak power as 1 kW or 2 kW, the spectra is quite flat with 10 dB fluctuation over 1300 nm optical bandwidth. As peak power increases ripples become more significant, rising up to 20 dB.

5.2 Arsenic selenide circular lattice PCF

In the case of As_2Se_3 glass, obtained ZDW at 2466 nm and pumping wavelength chosen as 2500 nm (Fig. 5.9a). Due to having high n_2 compared to As_2S_3 material, proposed C-PCF (As_2Se_3) offers γ of $14923 \text{ W}^{-1}\text{km}^{-1}$, which helps to make broader SCG in mid- IR region, and A_{eff} in the order of $4.042 \mu\text{m}^2$ (Fig. 5.10). The proposed C-PCF As_2Se_3 has negligible confinement loss up to wavelength 6000 nm (Fig. 5.11). By taking $\lambda = 2500 \text{ nm}$ as the pumping wavelength of the input pulse the calculated dispersion coefficient values of the Taylor expansion are $\beta_2 = -3.13 \times 10^{-2} \text{ ps}^2/\text{m}$, $\beta_3 = 3.087 \times 10^{-3} \text{ ps}^3/\text{m}$, $\beta_4 = -1.062 \times 10^{-5} \text{ ps}^4/\text{m}$, $\beta_5 = 7.1764 \times 10^{-8} \text{ ps}^5/\text{m}$, $\beta_6 = -5.3031 \times 10^{-10} \text{ ps}^6/\text{m}$, $\beta_7 = 4.8074 \times 10^{-12} \text{ ps}^7/\text{m}$, $\beta_8 = -3.7253 \times 10^{-14} \text{ ps}^8/\text{m}$, $\beta_9 = 1.1885 \times 10^{-16} \text{ ps}^9/\text{m}$ and $\beta_{10} = 1.0076 \times 10^{-17} \text{ ps}^{10}/\text{m}$.

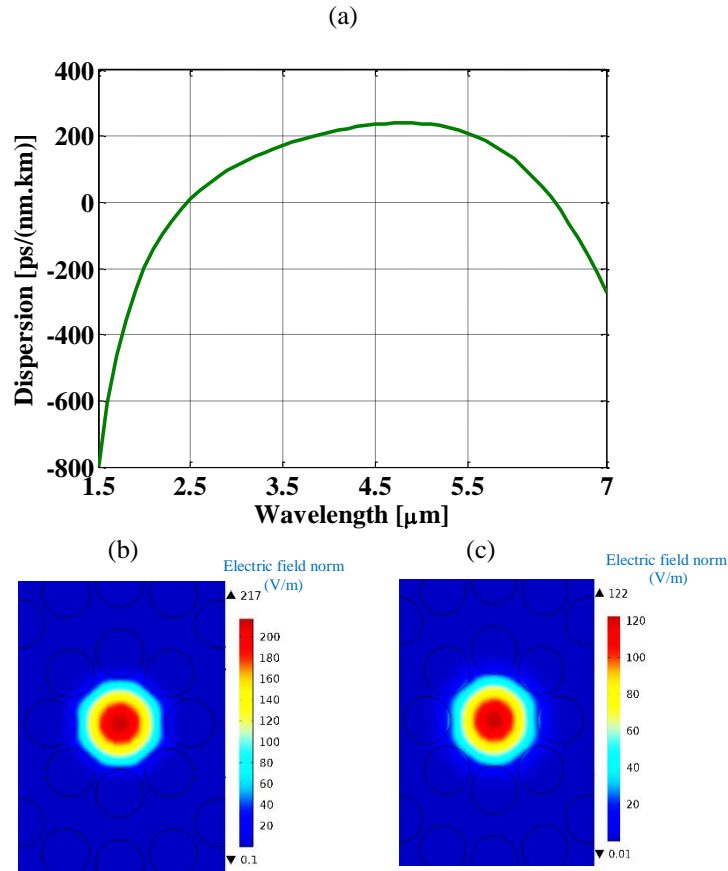


Fig. 5.9. (a) Dispersion curve as a function of wavelength by using optimized design parameters (As_2Se_3) (b) electric field distribution of C-PCF (As_2Se_3) at 1500 nm (c) electric field distribution of C-PCF (As_2Se_3) at 2500 nm.

During fabrication, there may be $\pm 2\%$ change in design parameters of proposed C-PCF [62]. That is why we perform tolerance analysis on proposed C-PCF by varying d (air hole's diameter). In As_2Se_3 C-PCF I vary air hole's diameter ($d = 1.2, 1.3$ and $1.4 \mu\text{m}$) keeping pitch fixed. From Fig. 5.12 it is clear that there is no such a significant change on dispersion curve while varying air hole's diameter; less sensitive to the structural parameters.

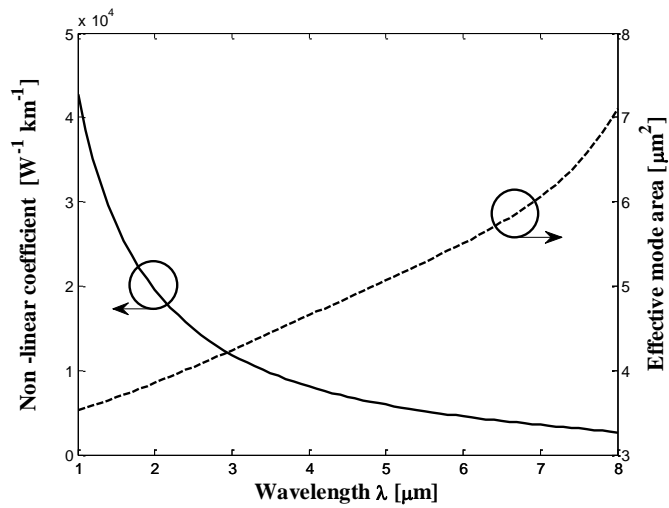


Fig. 5.10. Effective area and non-linear coefficient as a function of wavelength for materials As_2Se_3 .

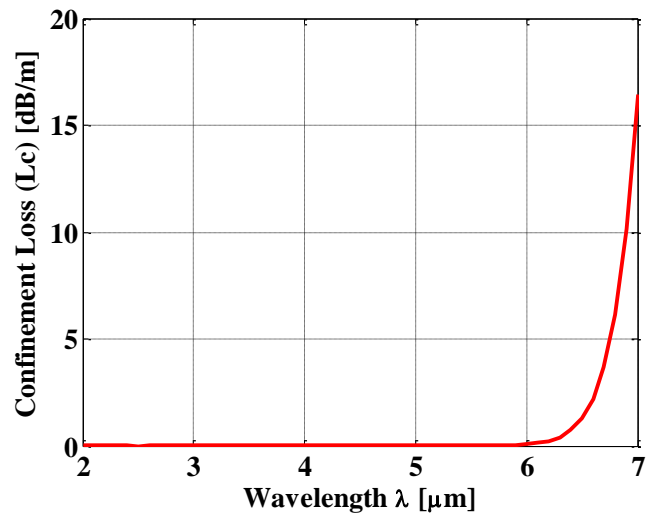


Fig. 5.11. Confinement loss as a function of wavelength (As_2Se_3).

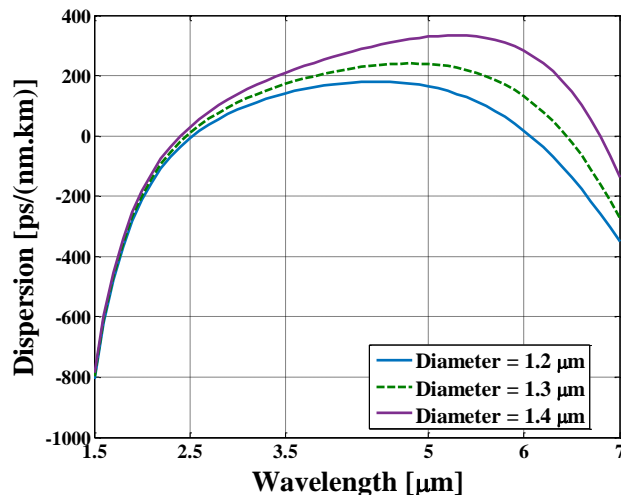


Fig. 5.12. Dispersion curve as a function of wavelength varying air hole's diameter in case of As_2Se_3 .

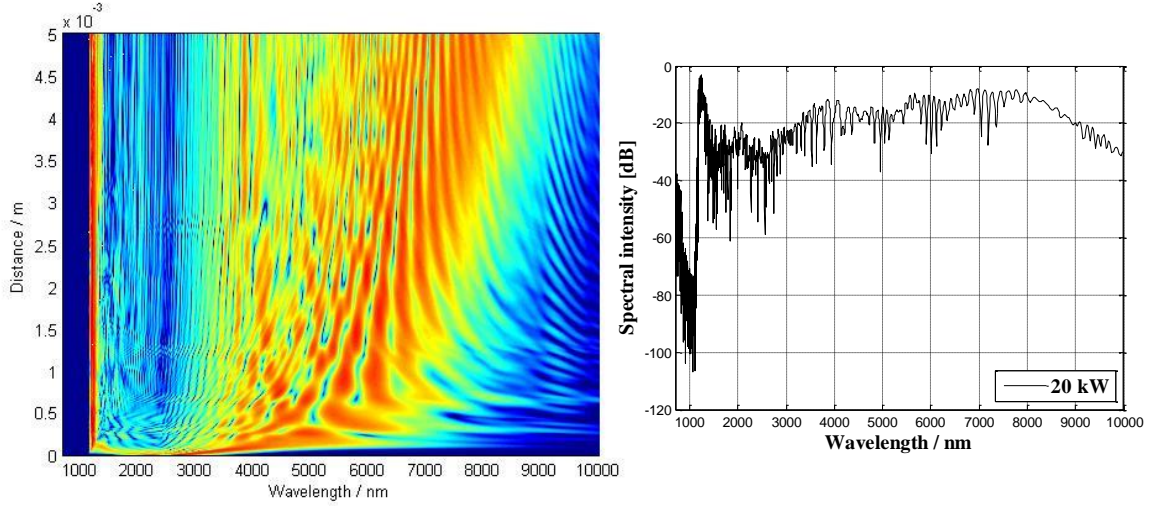


Fig. 5.13. Spectra of broadening in 0.5 cm long As_2Se_3 C-PCF using pump pulse with 20 kW peak power and $T_{FWHM} = 50$ fs.

Simulation parameters for SCG in the case of As_2Se_3 are then shown in Tab. 5.2. In simulation I have selected hyperbolic secant pulse as input pulse with $T_{FWHM} = 50$ fs and peak power 10 kW, 15 kW and 20 kW respectively. For pumping at 2500 nm, we can use mid-IR optical parametric oscillator (OPO), which is synchronously pumped by an erbium doped fiber laser, which operates in the 2.0 - 4.6 μm wavelength regime [63].

Spectral broadening up to 9000 nm is experienced when pumping with 20 kW peak power and $T_{FWHM} = 50$ fs (Fig. 5.13). From simulation results it is seen that by using peak power as 10 kW with $T_{FWHM} = 50$ fs, obtained spectral broadening about 5800 nm, from 1200 nm to 7000 nm (Fig. 5.14a). And by using peak power = 15 kW and $T_{FWHM} = 50$ fs, obtained spectral broadening is about 6600 nm, from 1200 nm to 7800 nm (Fig. 5.14b). L_{NL} and L_D of the proposed As_2Se_3 C-PCF are 6.70×10^{-6} m and 2.57×10^{-2} m respectively (using $P_0 = 10$ kW and $T_0 = 0.0284$ ps) at 2.50 μm pumping wavelength. Initial spectral broadening of input pulse lead by SPM though non-linear effect is dominant here ($L_{NL} < L_D$).

Table 5.2

Simulation parameters in the case of As_2Se_3

Parameters	Value
Pumping wavelength	2500 nm
Zero dispersion wavelength	2466 nm
Non – linear coefficient (γ)	At 2500 nm = $14923 \text{ W}^{-1}\text{km}^{-1}$
Fractional Raman contribution (f_R)	$f_R = 0.100$
Raman response parameters	$\tau_1 = 23.1$ fs, $\tau_2 = 195$ fs
Length of PCF (L_{PCF})	0.5 cm

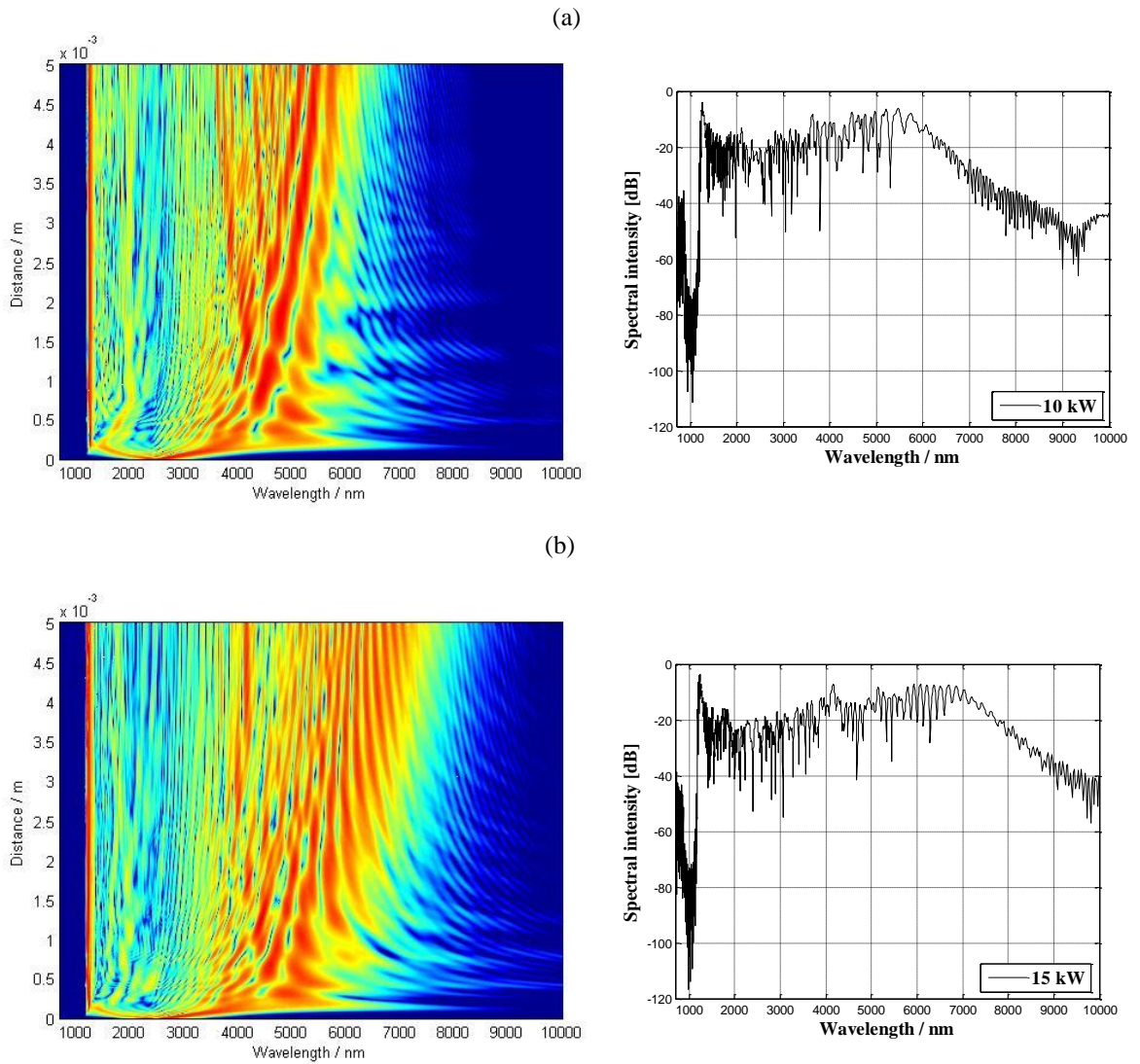


Fig. 5.14. Spectra of broadening in 0.5 cm long As_2Se_3 C-PCF using pump pulse with $T_{FWHM} = 50$ fs (a) 10 kW peak power (b) 15 kW peak power.

5.3 PBG-08 suspended core PCF (SC-PCF)

From Fig. 5.15 it is seen that the zero dispersion wavelengths (ZDW) of SC-PCF of three different core diameter are 1050 nm, 1330 nm and 1450 nm respectively. In accordance with the non-linear coefficients (γ) are $2442 \text{ W}^{-1}\text{km}^{-1}$, $566 \text{ W}^{-1}\text{km}^{-1}$ and $298.9 \text{ W}^{-1}\text{km}^{-1}$ respectively. The electric field distribution for different core diameter of SC-PCF are shown in Fig. 5.16.

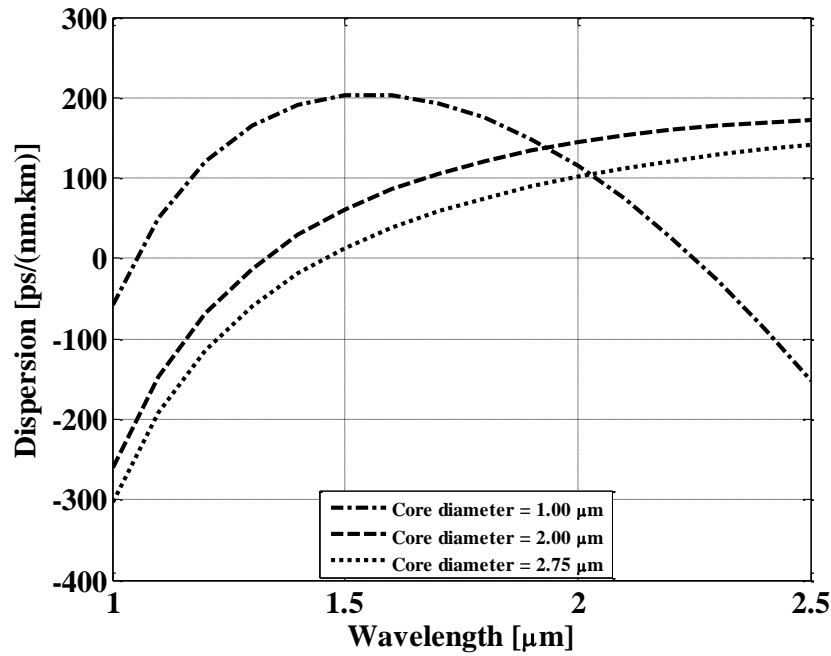


Fig. 5.15. Dispersion as a function of wavelength for different core diameter of SCF (PBG-08).

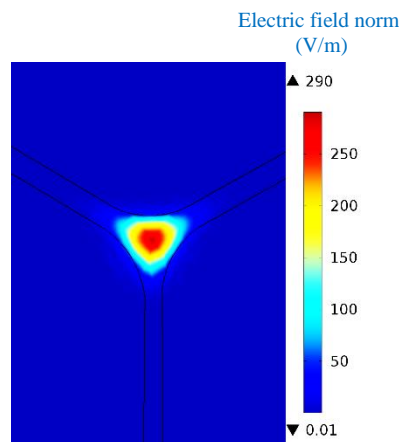


Fig. 5.16. Electric field distribution at 1350 nm for 2.00 μm core diameter SC-PCF.

Table 5.3

Summary of design and simulation parameters of SC-PCFs

Core diameter	Width of bridge	Radius of air hole	ZDW	Effective Area	Non-linear coefficient
1.00 μm	0.4 μm	24.5 μm	1050 nm	1.039 μm^2	2442 $\text{W}^{-1}\text{km}^{-1}$
2.00 μm	1.0 μm	24.0 μm	1330 nm	3.53 μm^2	566.0 $\text{W}^{-1}\text{km}^{-1}$
2.75 μm	1.6 μm	23.625 μm	1450 nm	5.83 μm^2	298.9 $\text{W}^{-1}\text{km}^{-1}$

For core diameter = 1.00 μm as get ZDW as 1050 nm, pumping wavelength chosen as 1060 nm in the anomalous dispersion regime and at pumping wavelength the calculated dispersion coefficient values of the Taylor expansion are $\beta_2=-7.5864\times 10^{-3}$ ps²/m, $\beta_3=3.7789\times 10^{-4}$ ps³/m, $\beta_4=-2.9065\times 10^{-7}$ ps⁴/m, $\beta_5=2.714\times 10^{-11}$ ps⁵/m, $\beta_6=3.8701\times 10^{-12}$ ps⁶/m, $\beta_7=-3.5983\times 10^{-14}$ ps⁷/m, $\beta_8=2.9253\times 10^{-16}$ ps⁸/m, $\beta_9=-2.4117\times 10^{-18}$ ps⁹/m and $\beta_{10}=2.0854\times 10^{-20}$ ps¹⁰/m respectively. Pumping wavelength chosen as 1350 nm for 2.00 μm core diameter in the anomalous dispersion regime and at pumping wavelength the calculated dispersion coefficient values of the Taylor expansion are $\beta_2=-9.2959\times 10^{-3}$ ps²/m, $\beta_3=4.0311\times 10^{-4}$ ps³/m, $\beta_4=-7.5249\times 10^{-7}$ ps⁴/m, $\beta_5=2.3442\times 10^{-9}$ ps⁵/m, $\beta_6=-7.9255\times 10^{-12}$ ps⁶/m, $\beta_7=2.7473\times 10^{-14}$ ps⁷/m, $\beta_8=-7.005\times 10^{-17}$ ps⁸/m, $\beta_9=-2.6924\times 10^{-19}$ ps⁹/m and $\beta_{10}=8.667\times 10^{-21}$ ps¹⁰/m respectively.

For core diameter = 2.75 μm , pumping wavelength chosen as 1550 nm and at pumping wavelength the calculated dispersion coefficient values of the Taylor expansion are $\beta_2=-3.37\times 10^{-2}$ ps²/m, $\beta_3=4.6237\times 10^{-4}$ ps³/m, $\beta_4=-1.1462\times 10^{-6}$ ps⁴/m, $\beta_5=4.4767\times 10^{-9}$ ps⁵/m, $\beta_6=-2.0628\times 10^{-11}$ ps⁶/m, $\beta_7=1.1153\times 10^{-13}$ ps⁷/m, $\beta_8=-6.9062\times 10^{-16}$ ps⁸/m, $\beta_9=4.8308\times 10^{-18}$ ps⁹/m and $\beta_{10}=-3.864\times 10^{-20}$ ps¹⁰/m respectively. In simulation I have used hyperbolic secant pulse as input pulse with peak power 1 kW, 5 kW and 10 kW with different pulse duration.

From Fig. 5.17a it is seen that in the case of 1.00 μm core diameter by using peak power 1 kW and $T_{FWHM} = 50$ fs, obtained spectral broadening about 750 nm from 700 nm to 1450 nm. In accordance with by using 10 kW peak power and 50 fs pulse duration (T_{FWHM}) 1400 nm spectral broadening is obtained from 800 nm to 2200 nm by using SCF of 2.00 μm core diameter (Fig. 5.17b) and spectral broadening about 1500 nm from 900 nm to 2400 nm for SCF of 2.75 μm core diameter (Fig. 5.18c). Non-linear length ($L_{NL}=1/\gamma P_0$) of the SCF for three different core diameter 1.00 μm , 2.00 μm and 2.75 μm are 8.19×10^{-5} m, 1.76×10^{-4} m, 3.34×10^{-4} m and dispersion length ($L_D=T_0^2/|\beta_2|$, $T_0= T_{FWHM}/1.763$) are 2.65×10^{-2} m, 8.6×10^{-2} m, 2.3×10^{-2} m respectively. The non-linear effect is dominant here because $L_{NL} < L_D$. The confinement loss of the analyzed SCF in all cases are negligible, so only material loss could have the dominant affect. Though short length of SCF is used here, so we can omit the effect of losses in broadening.

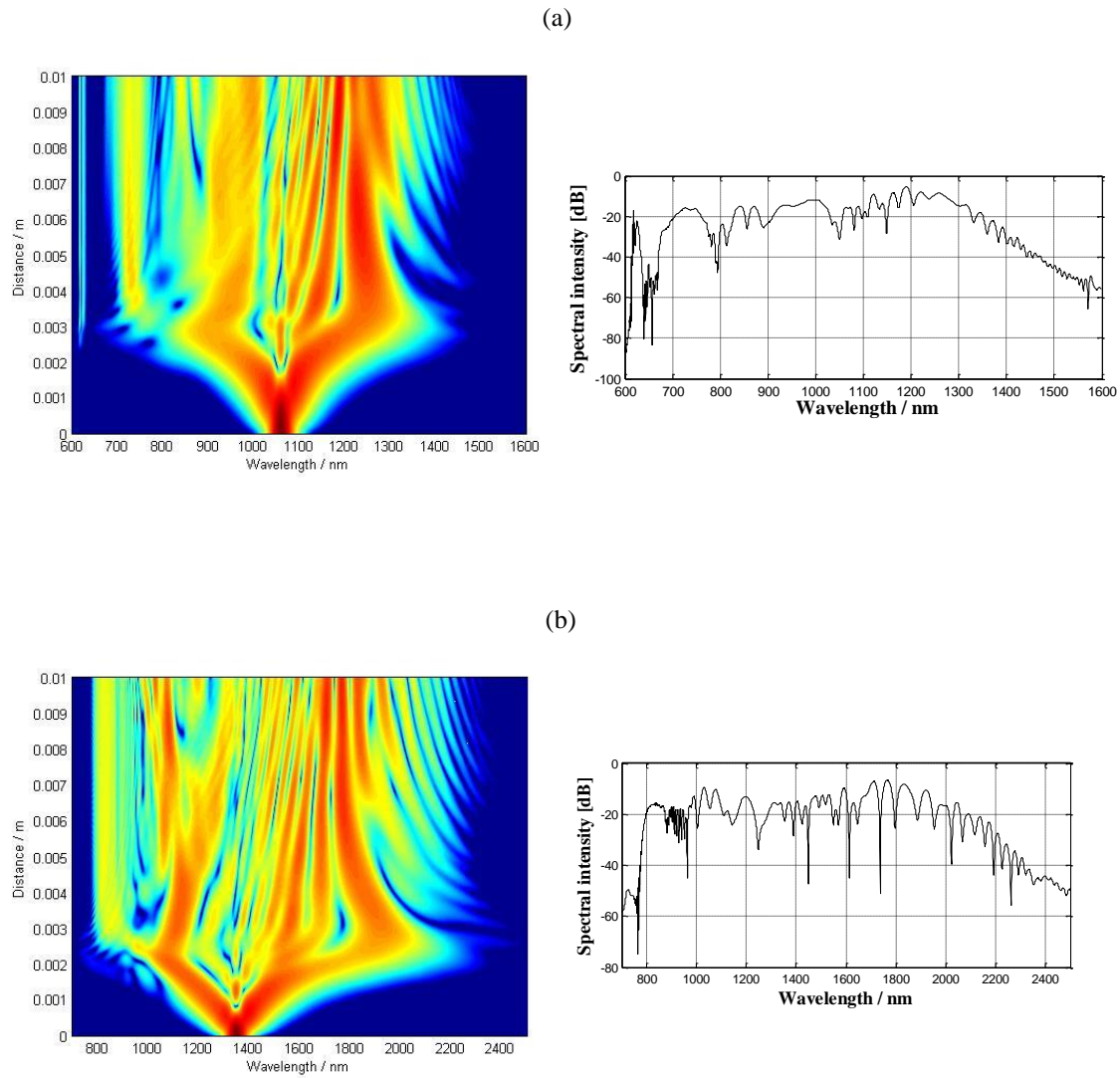


Fig. 5.17. SC spectra using (a) $P_{peak} = 1$ kW, $T_{FWHM} = 50$ fs for 1.00 μm core diameter SC-PCF (b) $P_{peak} = 10$ kW, $T_{FWHM} = 50$ fs for 2.00 μm core diameter SC-PCF.

By varying peak power (P_{peak}) from 1 kW to 10 kW with $T_{FWHM} = 50$ fs in the case of 2.75 μm core diameter SC-PCF is shown in Fig. 5.18. From figure it seen that though the broadening range up to 2500 nm, but there is a variation in intensity level as the fiber length is increasing. Which turns break the flatness of SC spectra and will induce remarkable fluctuations.

The effect of SC spectra by using different lengths (1 cm, 5 cm, 10 cm, 15 cm) by using $P_{peak} = 10$ kW are shown in Fig. 5.19.

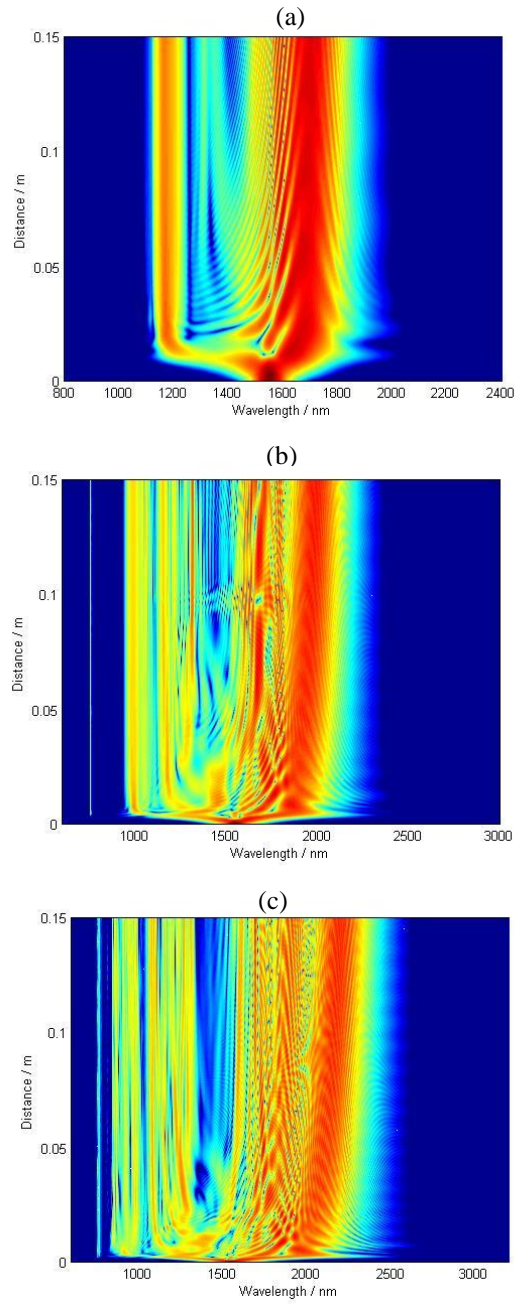


Fig. 5.18. SC spectra using (a) $P_{peak} = 1$ kW (b) $P_{peak} = 5$ kW (c) $P_{peak} = 10$ kW, $T_{FWHM} = 50$ fs for 2.75 μm core diameter SC-PCF.

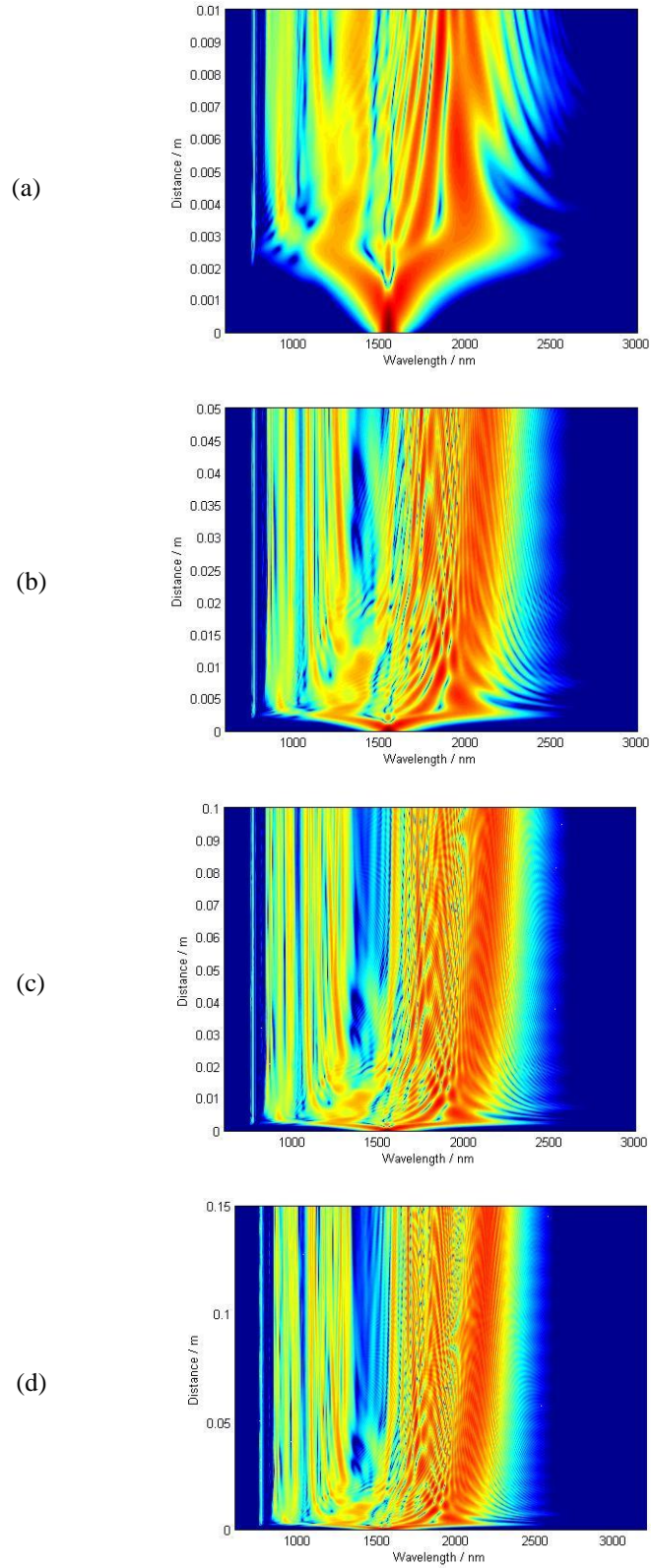


Fig. 5.19. SC spectra using $P_{peak} = 10$ kW, $T_{FWHM} = 50$ fs for 2.75 μ m core diameter SC-PCF of length (a) 1 cm (b) 5 cm (c) 10 cm (d) 15 cm.

5.4 PBG-08 hexagonal PCF

In this section I have analyzed hexagonal PCF made of PBG-08 glass material having core diameter of 2.64 μm . From Fig. 5.20 it is seen that the zero dispersion wavelengths (ZDW) of H-PCF is 1555 nm. Effective area and non-linear coefficient are 4.613 μm^2 and 375.4327 $\text{W}^{-1} \text{km}^{-1}$ at pumping wavelength 1560 nm (see Fig. 5.21b). The electric field distribution of H-PCF at 1560 nm is shown in Fig. 5.21a.

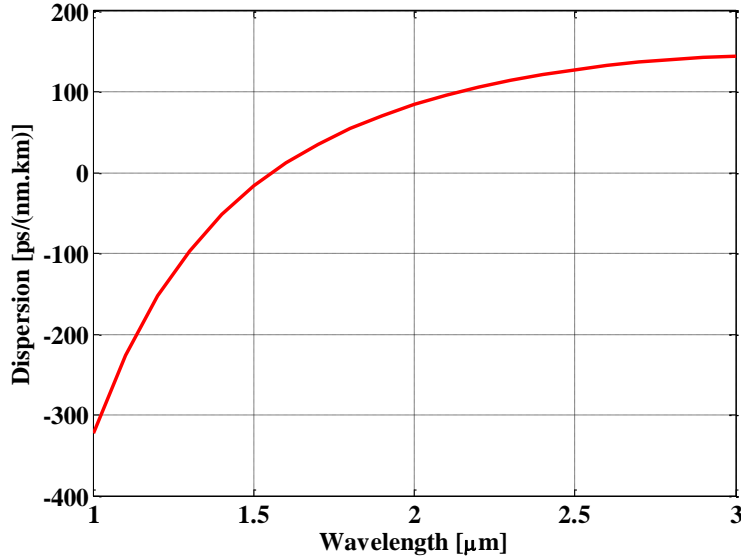


Fig. 5.20. Dispersion as a function of wavelength in case of H-PCF.

As ZDW is obtained at 1555 nm, chose pumping wavelength chosen as 1560 nm in the anomalous dispersion regime and at pumping wavelength the calculated dispersion coefficient values of the Taylor expansion are $\beta_2 = -1.4481 \times 10^{-3} \text{ ps}^2/\text{m}$, $\beta_3 = 4.7000 \times 10^{-4} \text{ ps}^3/\text{m}$, $\beta_4 = -1.0898 \times 10^{-6} \text{ ps}^4/\text{m}$, $\beta_5 = 3.6563 \times 10^{-9} \text{ ps}^5/\text{m}$, $\beta_6 = -1.562 \times 10^{-11} \text{ ps}^6/\text{m}$, $\beta_7 = 7.2007 \times 10^{-14} \text{ ps}^7/\text{m}$, $\beta_8 = -2.7078 \times 10^{-16} \text{ ps}^8/\text{m}$, $\beta_9 = -6.1724 \times 10^{-19} \text{ ps}^9/\text{m}$ and $\beta_{10} = 3.8863 \times 10^{-20} \text{ ps}^{10}/\text{m}$ respectively. In simulation I have used hyperbolic secant pulse as input pulse with peak power of 10 kW, 5 kW and 1 kW with $T_{FWHM} = 50 \text{ fs}$ pulse duration and their corresponding broadening range are 1400 nm, 1100 nm and 700 nm respectively (see Fig. 5.22). The effect of changing pulse duration on SC spectra are shown in Fig. 5.23.

Table 5.4

Summary of simulation parameters

Zero dispersion wavelength	1555 nm
Non-linear coefficient (γ)	375.4327 $\text{W}^{-1} \text{km}^{-1}$
Effective area (A_{eff})	4.613 μm^2
L_{PCF}	15 cm

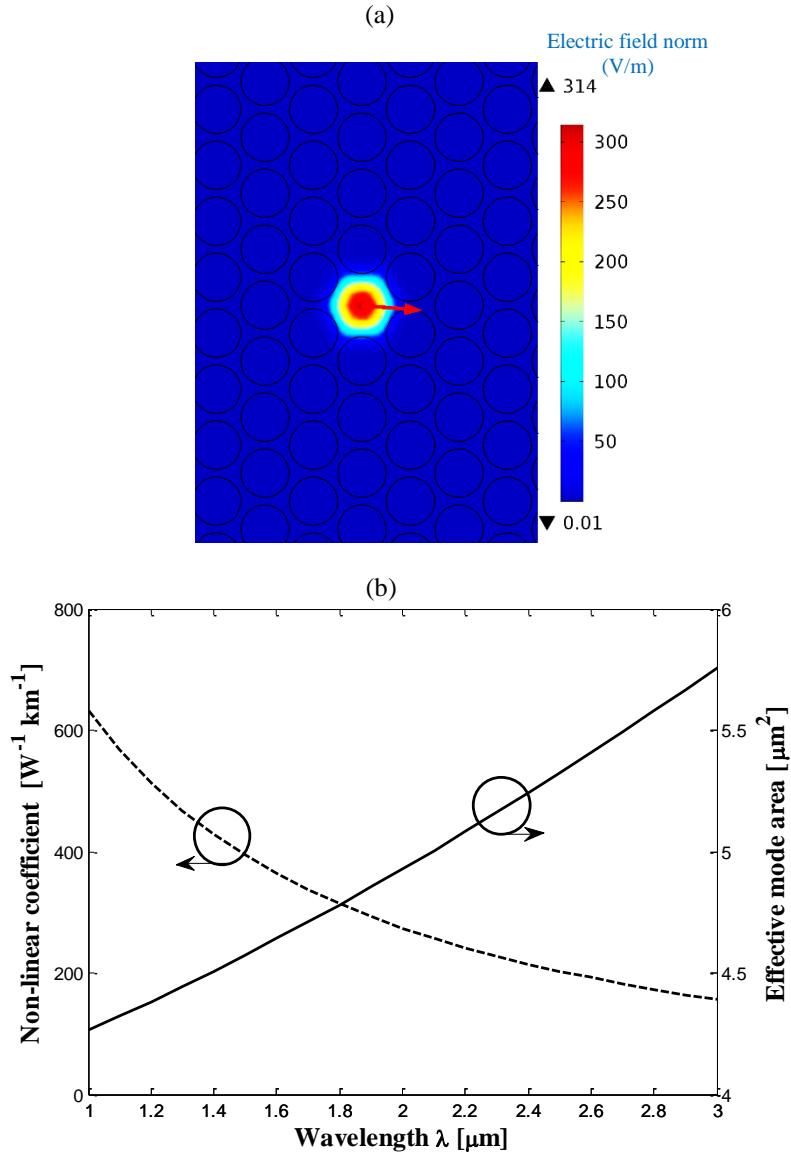


Fig. 5.21. (a) Electric field distribution of H-PCF at 1560 nm (b) effective area and non-linear coefficient as a function of wavelength in case of H-PCF.

Table 5.5
Broadening range by varying peak power (H-PCF)

Pulse duration	Peak power	Bandwidth	Broadening range
$T_{FWHM}= 50$ fs	10 kW	1400 nm	1000 nm – 2400 nm
$T_{FWHM}= 50$ fs	5 kW	1100 nm	1100 nm – 2200 nm
$T_{FWHM}= 50$ fs	1 kW	700 nm	1300 nm – 2000 nm

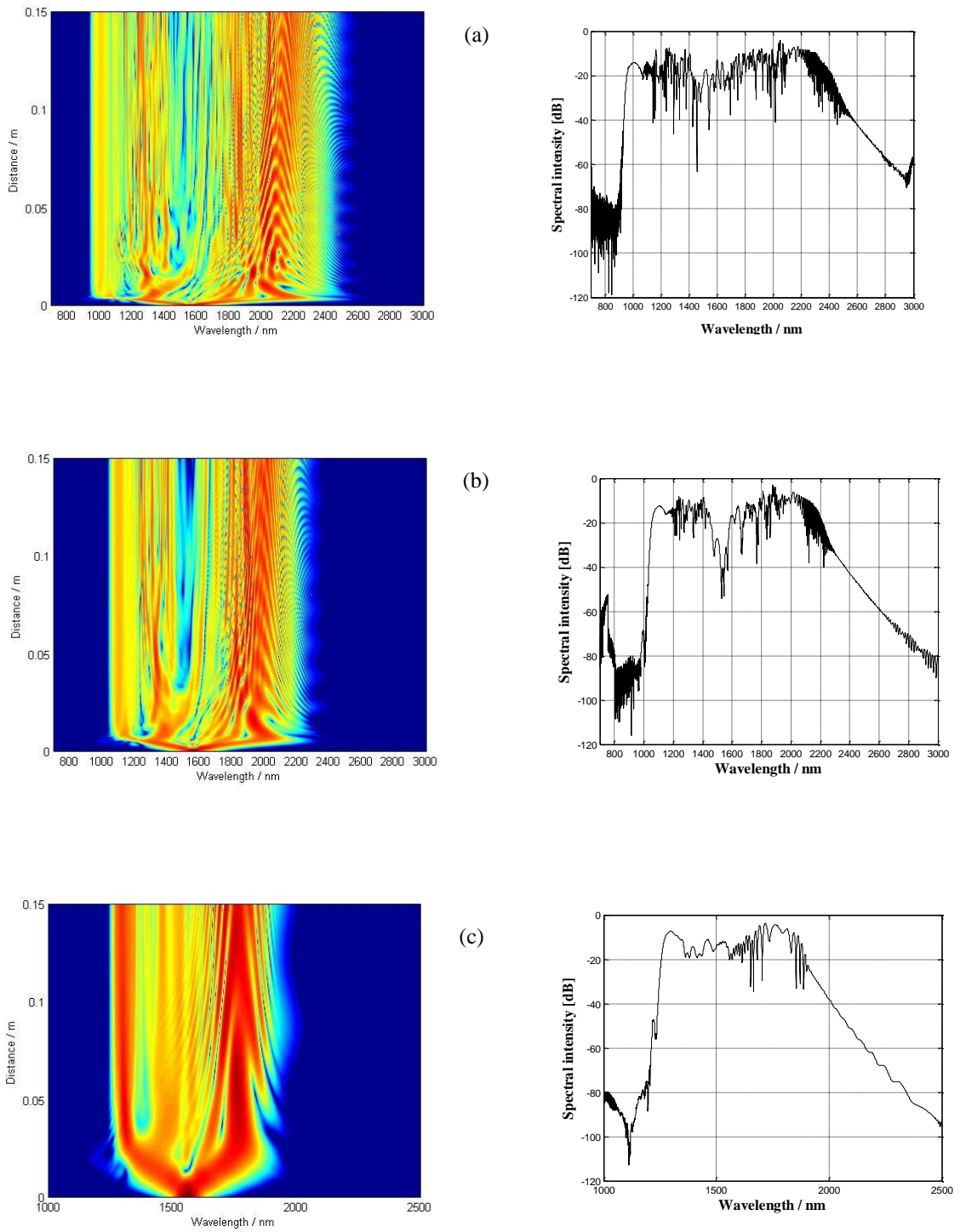


Fig. 5.22. In the case of H-PCF, SC spectra using $T_{FWHM} = 50$ fs and P_{peak} as (a) 10 kW (b) 5 kW (c) 1 kW.

From Fig. 5.23 is seen that as the pulsed duration is increased broadening range is kept same with lower intensity level. Moreover change in peak power has some significant change in broadening as shown in Fig 5.22. Compared to SC-PCF (2.75 μm) as shown in last section, SC spectra has no such large fluctuations in H-PCF.

Table 5.6
Broadening range by varying pulse duration ((H-PCF))

Peak power	Pulse duration	Bandwidth	Broadening range
5 kW	$T_{FWHM} = 50$ fs	1100 nm	1100 nm – 2200 nm
5 kW	$T_{FWHM} = 100$ fs	1100 nm	1100 nm – 2200 nm

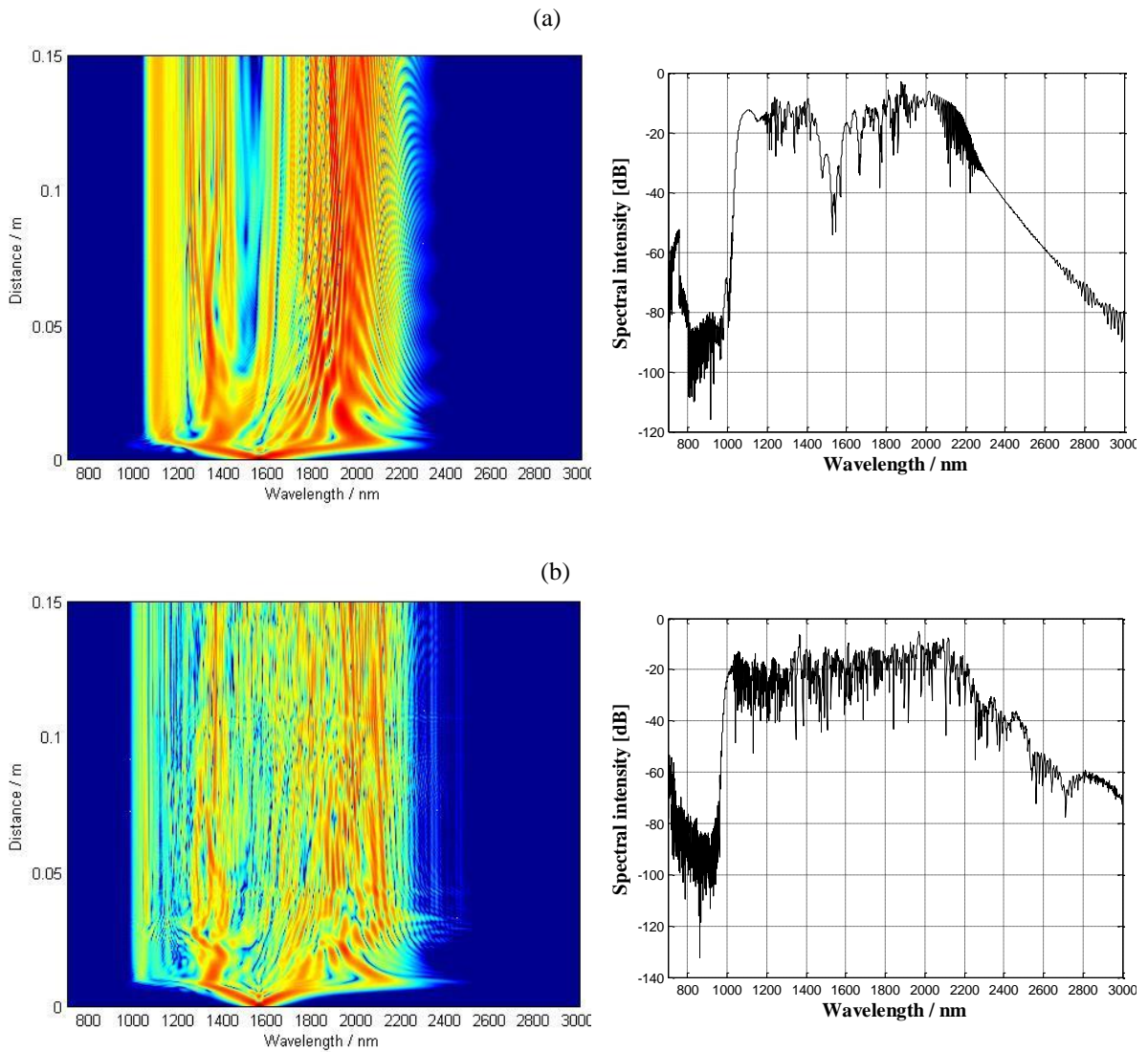
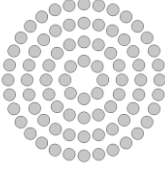
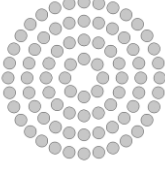
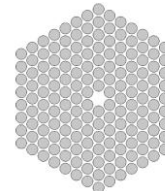
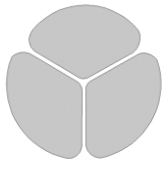


Fig. 5.23. In the case of H-PCF, SC spectra using $P_{peak} = 5$ kW with (a) $T_{FWHM} = 50$ fs (b) $T_{FWHM} = 100$ fs.

5.5 Comparison of different designs of PCF

Table 5.7
Comparison table of broadening range in different designs

Name	Design	Nonlinear Coefficient (γ)	Pumping wavelength	Zero Dispersion Wavelength	Peak power & pulse duration	Broadening range
Circular PCF Material : As_2Se_3	 Core Diameter: 2.5 μm	14923 $\text{W}^{-1}\text{km}^{-1}$	2500 nm	2466 nm	$P_{peak} = 20 \text{ kW}$ $T_{FWHM} = 50 \text{ fs}$	1000 nm to 9000 nm B.W: 8000 nm
Circular PCF Material : As_2S_3	 Core Diameter: 2.5 μm	2362 $\text{W}^{-1}\text{km}^{-1}$	2000 nm	1985 nm	$P_{peak} = 10 \text{ kW}$ $T_{FWHM} = 50 \text{ fs}$	1000 nm to 4000 nm B.W: 3000 nm
Hexagonal PCF Material : PBG-08	 Core Diameter: 2.64 μm	375.43 $\text{W}^{-1} \text{ km}^{-1}$	1560 nm	1555 nm	$P_{peak} = 10 \text{ kW}$ $T_{FWHM} = 50 \text{ fs}$	900 nm to 2400 nm B.W: 1500 nm
Suspended core PCF Material : PBG-08	 Core Diameter: 2.75 μm	298.9 $\text{W}^{-1}\text{km}^{-1}$	1550 nm	1450 nm	$P_{peak} = 10 \text{ kW}$ $T_{FWHM} = 50 \text{ fs}$	900 nm to 2500 nm B.W: 1600 nm

6. Conclusion and future work

6.1 Conclusion

I have presented the design of the circular lattice photonic crystal fiber with 2.5 μm core diameter based on chalcogenide glass. Dispersion profile was tailored for broadband MIR supercontinuum generation. Pumps were allocated at 2000 nm and 2500 nm for arsenic-sulfide and arsenic-selenide respectively. Numerical studies showed that the proposed C-PCFs are suitable for mid-IR supercontinuum generation, in the case of As_2S_3 and As_2Se_3 by employing only 5 mm long C-PCF I obtained spectral broadening of 3000 nm and 8000 nm respectively. These proposed C-PCFs could be suitable candidates for different applications such as spectroscopy, pulse compression, gas sensing and various nonlinear applications. The major advantage of the proposed design represents manufacturing simplicity and tolerance to manufacturing imperfections.

From analysis of supercontinuum generation in SC-PCF and H-PCF it is seen that spectral broadening from 800 nm to 2400 nm could be achievable by using 2.75 μm core diameter SC-PCF with pumping wavelength at 1550 nm. By using core diameter of 2.64 μm of H-PCF we could get the quit same broadening in SC as SC-PCF. But compared to SC-PCF, the H-PCF shows SC spectra with good flatness when using 10 kW peak power.

From my analysis it has been proven that chalcogenide glass, especially As_2Se_3 , is a suitable candidate for high range of SC spectra such as up to 10 μm . PBG-08 glass PCF, as a soft-glass, also exhibits spectral broadening over 1500 nm, when pumped at 1550 nm.

6.2 Recommendations for future work

- I have analyzed SCG by using anomalous dispersion regime. Some significant ripples at high peak power in SC spectra were observed. In future it will be of great interest to achieve flat SC spectra in MIR by extending the present work of this thesis.
- Analysis of SCG by selecting pumping region at normal dispersion regime.
- I have analyzed SCG by using circular PCF, hexagonal PCF, suspended core PCF. It is also interesting to use spiral PCF, square PCF etc. and in the further investigation as a host material can be used such as tellurite glass, SF57, other chalcogenide glasses, etc.

References

- [1] J. A. Buck, *Fundamentals of Optical Fibers*, Wiley, Hoboken, New Jersey (2004).
- [2] T. A. Birks *et al.*, “Endlessly single-mode photonic crystal fibre”, *Opt. Lett.* 22 (13), 961 (1997).
- [3] A. Ortigosa-Blanch *et al.*, “Highly birefringent photonic crystal fibres”, *Opt. Lett.* 25 (18), 1325 (2000).
- [4] P. St. J. Russell, “Photonic crystal fibers,” *Science*, vol. 299, pp. 358-362, 2003.
- [5] J. C. knight, “Photonic crystal fibers,” *Nature*, vol. 424, pp. 847–851, 2003.
- [6] J. C. Knight, T. A. Birks, P. S. J. Russell, and D. M. Atkin, “All-silica single-mode optical fiber with photonic crystal cladding,” *Opt. Lett.*, vol. 21, pp. 1547–1549, 1996.
- [7] T.A. Birks, J.C. Knight, B.J. Mangan, and P.St.J. Russell, “Photonic crystal fibers: An endless variety,” *IEICE Trans. Electron.*, E84-C, pp. 585-592, 2001.
- [8] R. F. Cregan *et al.*, “Single-mode photonic band gap guidance of light in air”, *Science* 285, 1537 (1999).
- [9] J.M. Dudley, G. Genty, and S. Coen, “Supercontinuum generation in photonic crystal fiber,” *Rev. Mod. Phys.*, vol. 78, pp. 1135, 2006.
- [10] R.R. Alfano, S.L. Shapiro, Emission in the region 4000 to 7000 angstrom via four-photon coupling in glass, *Phys. Rev. Lett.* 24 (1970) 584–587.
- [11] J.S. Sanghera, L. B. Shaw, and I.D. Aggarwal, “Chalcogenide glass-fiber-based Mid-IR sources and applications,” *IEEE Journal of Selected Topics in Quantum Electronics*, vol. 15, pp. 114-119, 2009.
- [12] G. Qin, X. Yan, C. Kito, M. Liao, C. Chaudhari, T. Suzuki, and Y. Ohishi, “Ultrabroadband supercontinuum generation from ultraviolet to 6.28 μm in a fluoride fiber,” *Appl. Phys. Lett.*, vol. 95, pp. 161103, 2009.
- [13] N. Granzow, S.P. Stark, M.A. Schmidt, A.S. Tverjanovich, L. Wondraczek, and P. St. J. Russell, “Supercontinuum generation in chalcogenide-silica step-index fibers,” *Opt. Express*, vol. 19, 2011.
- [14] D. Buccoliero, H. Steffensen, O. Bang, H. Ebendorff-Heidepriem, and T. M. Monro, “Thulium pumped high power supercontinuum in loss determined optimum lengths of tellurite photonic crystal fiber,” *Appl. Phys. Lett.*, vol. 97, pp. 061106, 2010.
- [15] M.S. Liao, X. Yan, Z.C. Duan, T. Suzuki, and Y. Ohishi, “Tellurite photonic nanostructured fiber,” *J. Lightwave Technol.*, vol. 29, pp. 1018–1025, 2011.
- [16] T.L. Cheng, W.Q. Gao, H. Kawashima, D.H. Deng, M.S. Liao, M. Matsumoto, T. Misumi, T. Suzuki, and Y. Ohishi, “Widely tunable second-harmonic generation in a chalcogenide–tellurite hybrid optical fiber,” *Opt. Lett.*, vol. 39, pp. 2145–2147, 2014.
- [17] L. Liu, G. Qin, Q. Tian, D. Zhao, and W. Qin, “Numerical investigation of mid-infrared supercontinuum generation up to 5 μm in single mode fluoride fiber,” *Opt. Express*, vol. 19, pp. 10041–10048, 2011.
- [18] R.T. White and T.M. Monro, “Cascaded Raman shifting of high-peak-power nanosecond pulses in As_2S_3 and As_2Se_3 optical fibers,” *Opt. Lett.*, vol. 36, pp. 2351–2353, 2011.
- [19] Christian Rosenberg Petersen, Uffe Møller, Irnis Kubat, Binbin Zhou, Sune Dupont, Jacob Ramsay, Trevor Benson, Slawomir Sujecki, Nabil AbdelMoneim, Zhuoqi Tang, David Furniss, Angela Seddon, and Ole Bang,

- “Mid-infrared supercontinuum covering the 1.4–13.3 μm molecular fingerprint region using ultra-high NA chalcogenide step-index fibre,” *Nat. Photonics*, vol. 8, pp. 830–834, 2014.
- [20] X. Feng, A. K. Mairaj, D. W. Hewak, and T. M. Monro, “Nonsilica glass for holey fibers,” *J. Lightwave Technol.*, vol. 23, pp. 2046–2054, 2005.
- [21] J.H. Price, T.M. Monro, H. Ebendorff-Heidepriem, F. Poletti, P. Horak, V. Finazzi, J.Y.Y. Leong, P. Petropoulos, J.C. Flanagan, G. Brambilla, X. Feng, and D.J. Richardson, “Mid-IR supercontinuum generation from non-silica microstructured optical fibers,” *IEEE J. Sel. Top. Quant. Electron.*, vol. 3, pp. 738–749, 2007.
- [22] J.H.V. Price and D.J. Richardson, “Supercontinuum generation and nonlinearity in soft glass fibers,” in: J.M. Dudley, R. Taylor (Eds.), *Supercontinuum Generation in Optical Fibers*, Cambridge University Press (CUP), Cambridge, pp. 82–118, 2010.
- [23] I. Hartl, X.D. Li, C. Chudoba, R.K. Ghanta, T.H. Ko, J.G. Fujimoto, J.K. Ranka, and R.S. Windeler, “Ultrahigh-resolution optical coherence tomography using continuum generation in an air—Silica microstructure optical fiber,” *Opt. Lett.*, vol. 26, no. 9, pp. 608–610, 2001.
- [24] B. Schenkel, R. Paschotta, and U. Keller, “Pulse compression with supercontinuum generation in microstructure fibers,” *J. Opt. Soc. Amer. B*, vol. 22, no. 3, pp. 687–693, 2005.
- [25] S. Moon and D. Y. Kim, “Ultra-high-speed optical coherence tomography with a stretched pulse supercontinuum source,” *Opt. Exp.*, vol. 14, no. 24, pp. 11575–11584, 2006.
- [26] A F.-L. Hong, K. Minoshima, A. Onae, H. Inaba, H. Takada, A. Hirai, H. Matsumoto, T. Sugiura, and M. Yoshida, “Broad-spectrum frequency comb generation and carrier-envelope offset frequency measurement by second-harmonic generation of a mode-locked fiber laser,” *Opt. Lett.*, vol. 28, pp. 1516, 2003.
- [27] H. Kano and H. Hamaguchi, “Femtosecond coherence anti-stokes Raman scattering spectroscopy using supercontinuum generated from a photonic crystal fiber,” *Appl. Phys. Lett.*, vol. 85, pp. 4298, 2004.
- [28] N. Nishizawa, Y. Chen, P. Hsiung, E.P. Ippen, and J.G. Fujimoto, “Real-time, ultrahigh resolution, optical coherence tomography with an all-fiber, femtosecond fiber laser continuum at 1.5 microm”, *Opt. Lett.*, vol. 29, pp. 2846-2848, 2004.
- [29] Fiber Lasers edited by Oleg G. Okhotnikov, page 69.
- [30] Than Singh Saini, A. Kumar, and R K Sinha, "Broadband Mid-Infrared Supercontinuum Spectra Spanning 2–15 μm Using As_2Se_3 Chalcogenide Glass Triangular-Core Graded-Index Photonic Crystal Fiber," *J. Lightwave Technol.*, vol. 33, pp. 3914-3920, 2015.
- [31] W. Yuan, “2-10 μm mid-infrared supercontinuum generation in As_2Se_3 photonics crystal fiber,” *Laser Phys. Lett.*, vol. 10, pp. 095107, 2013.
- [32] P. Domachuk, N. A. Wolchover, M. Cronin-Golomb, A. Wang, A. K. George, C.M.B. Cordeiro, J.C. Knight, and F. G. Omenetto, "Over 4000 nm Bandwidth of Mid-IR Supercontinuum Generation in sub-centimeter Segments of Highly Nonlinear Tellurite PCFs," *Opt. Express* 16, 7161-7168 (2008).
- [33] I. Savelli, O. Mouawad, J. Fatome, B. Kibler, F. Désévéday, G. Gadret, J-C Jules, P-Y Bony, H. Kawashima, W. Gao, T. Kohoutek, T. Suzuki, Y. Ohishi, and F. Smektala, "Mid-infrared 2000-nm bandwidth

- supercontinuum generation in suspended-core microstructured Sulfide and Tellurite optical fibers," *Opt. Express* 20, 27083-27093 (2012).
- [34] Zhu Xing-Ping, Li Shu-Guang, Du Ying, Han Ying, Zhang Wen-Qi, Ruan Yin-Lan, Heike Ebendorff-Heidepriem, Shahraam Afshar, and Tanya M. Monroe, "High stability supercontinuum generation in lead silicate SF57 photonic crystal fibers," *Chin. Phys. B* Vol. 22, No. 1, 014215, (2013).
- [35] K Porsezian, R Vasantha Jayakantha Raja, "Soliton fission and supercontinuum generation in photonic crystal fibre for optical coherence tomography application," *Pramana- journal of physics*, November 2015, Volume 85, Issue 5, pp 993-1007.
- [36] <https://en.wikipedia.org/wiki/Supercontinuum>
- [37] Tingye Li, Alan E. Willner, Ivan Kaminow, "Optical Fiber Telecommunications VA: Components and Subsystems" Page no- 505.
- [38] Robert Thomson, "Ultrafast nonlinear fiber optics and Supercontinuum generation", Page No- 181.
- [39] G. P. Agrawal, *Nonlinear Fiber Optics*. New York: NY, USA, Springer, 2000.
- [40] Ji Cheng, Jennifer H. Lee, Ke Wang, Chris Xu, Kim G. Jespersen, Martin Garmund, Lars Grüner-Nielsen, and Dan Jakobsen, "Generation of Cerenkov radiation at 850 nm in higher-order-mode fiber," *Opt. Express* 19, 8774-8780 (2011).
- [41] Weiqing Gao, Mohammed El Amraoui, Meisong Liao, Hiroyasu Kawashima, Zhongchao Duan, Dinghuan Deng, Tonglei Cheng, Takenobu Suzuki, Younès Messaddeq, and Yasutake Ohishi, "Mid-infrared supercontinuum generation in a suspended-core As₂S₃ chalcogenide microstructured optical fiber," *Opt. Express*, vol. 21, pp. 9573-9583, 2013.
- [42] M. El-Amraoui, J. Fatome, J. C. Jules, B. Kibler, G. Gadret, C. Fortier, F. Smektala, I. Skripatchev, C. F. Polacchini, Y. Messaddeq, J. Troles, L. Brilland, M. Szpulak, and G. Renversez, "Strong infrared spectral broadening in low-loss As-S chalcogenide suspended core microstructured optical fibers," *Opt. Express*, vol. 18 no. 5, pp. 4547-4556, 2010.
- [43] Bora Ung and Maksim Skorobogatiy, "Chalcogenide microporous fibers for linear and nonlinear applications in the mid-infrared," *Opt. Express*, vol. 18, pp. 8647-8659, 2010.
- [44] J. Hu, C. R. Menyuk, L. B. Shaw, J. S. Sanghera, and I. D. Aggarwal, "Raman response function and supercontinuum generation in chalcogenide fiber", presented at the *Conference on Lasers and Electro-Optics (CLEO)*, San Jose, CA, Paper CMDD2, 2008.
- [45] Grzegorz Sobon, Mariusz Klimczak, Jaroslaw Sotor, Karol Krzempek, Dariusz Pysz, Ryszard Stepień, Tadeusz Martynkien, Krzysztof M. Abramski, and Ryszard Buczynski, "Infrared supercontinuum generation in soft-glass photonic crystal fibers pumped at 1560 nm," *Opt. Mater. Express* 4, 7-15, 2014.
- [46] K. Saitoh and M. Koshiba, "Full-vectorial imaginary-distance beam propagation method based on a finite element scheme: Application to photonic crystal fibers," *IEEE J. Quantum Electron.*, vol. 38, no. 7, pp. 927-933, 2002.
- [47] K. Suzuki, H. Kubota, S. Kawanishi, M. Tanaka, and M. Fujita, "Optical Properties of Low Loss Polarization Maintaining Photonic Crystal Fibre," *Opt. Express*, vol. 9, no. 13, pp. 676-680, 2001.

- [48] Liu Shuo and Li Shu-Guang, "Numerical analysis of photonic crystal fiber with chalcogenide core tellurite cladding composite microstructure", *Chin. Phys. B*, vol. 22, no. 7, pp. 074206, 2013.
- [49] Bora Ung and Maksim Skorobogatiy, "Chalcogenide microporous fibers for linear and nonlinear applications in the mid-infrared," *Opt. Express*, vol. 18, pp. 8647-8659, 2010.
- [50] Amorphous Materials, "AMTIR-2: Arsenic Selenide Glass As-Se," Amorphous Materials Inc., 2009. (www.amorphousmaterials.com)
- [51] Jiří Kaňka, "Design of photonic crystal fibers with highly nonlinear glasses for four-wave-mixing based telecom applications," *Opt. Express*, vol. 16, pp. 20395-20408, 2008.
- [52] R. Buczynski, H. Bookey, M. Klimczak, D. Pysz, R. Stepien, T. Martynkien, J. E. McCarthy, A. J. Waddie, A. K. Kar and M. R. Taghizadeh, "Two Octaves Supercontinuum Generation in Lead-Bismuth Glass Based Photonic Crystal Fiber," *Materials* 2014, 7, 4658-4668
- [53] Jacek Swiderski, "High-power mid-infrared supercontinuum sources: Current status and future perspectives," *Progress in Quantum Electronics* 38 (2014) 189– 235.
- [54] R. Thapa, D. Rhonehouse, D. Nguyen, K. Wiersma, C. Smith, J. Zong, A. Chavez-Pirson, in: David H. Titterton, Mark A. Richardson, Robert J. Grasso, Harro Ackermann, Willy L. Bohn (Eds.), *Proceedings of SPIE, Technologies for Optical Countermeasures X; and High-Power Lasers 2013: Technology and Systems*, vol. 8898, 2013, p. 889808.
- [55] J.S. Sanghera, L.B. Shaw, P. Pureza, V.Q. Nguyen, D. Gibson, L. Busse, I.D. Aggarwal, C.M. Florea, F.H. Kung, *Int. J. Appl. Glass Sci.* 1 (2010) 296–308.
- [56] M. Saad, in: Bishnu P. Pal (ed.), *Proceedings of SPIE, Passive Components and Fiber-Based Devices VIII*, vol. 8307, 2011, p. 83070N.
- [57] J. A. Savage, "Materials for infrared fibre optics," *Mater. Sci. Eng. Rep.* 2(3), 99–137 (1987).
- [58] J. A. Harrington, *Infrared Fibers and Their Applications* (SPIE-The International Society for Optical Engineering, 2004).
- [59] Chen Wei, Xiushan Zhu, Robert A. Norwood, Feng Song, and N. Peyghambarian, "Numerical investigation on high power mid-infrared supercontinuum fiber lasers pumped at 3 μm ," *Opt. Express* 21, 29488-29504 (2013).
- [60] J. Swiderski, M. Michalska, and G. Maze, "Mid-IR supercontinuum generation in a ZBLAN fiber pumped by a gain-switched mode-locked Tm-doped fiber laser and amplifier system," *Opt. Express*, vol. 21, 2013.
- [61] O. P. Kulkarni, V. V. Alexander, M. Kumar, M. J. Freeman, M. N. Islam, F. L. Terry, Jr., M. Neelakandan, and A. Chan, "Supercontinuum generation from ~ 1.9 to 4.5 μm in ZBLAN fiber with high average power generation beyond 3.8 μm using a thulium-doped fiber amplifier," *J. Opt. Soc. Am. B*, vol. 28, pp. 2486, 2011.
- [62] F. Poletti, V. Finazzi, T. M. Monro, N. G. R. Broderick, V. Tse and D. J. Richardson, "Inverse design and fabrication tolerances of ultraflattened dispersion holey fibers", *Opt. Express*, vol.13, pp. 3728–3736, 2005.
- [63] Alireza Marandi, Charles W. Rudy, Victor G. Plotnichenko, Evgeny M. Dianov, Konstantin L. Vodopyanov and, Robert L. Byer, "Mid-infrared supercontinuum generation in tapered chalcogenide fiber for producing octave-spanning frequency comb around 3 μm ," *Opt. Express*, vol. 20, pp. 24218-24225, 2012.